



THE UNIVERSITY OF  
**WAIKATO**  
*Te Whare Wānanga o Waikato*

Research Commons

<http://researchcommons.waikato.ac.nz/>

## Research Commons at the University of Waikato

### Copyright Statement:

The digital copy of this thesis is protected by the Copyright Act 1994 (New Zealand).

The thesis may be consulted by you, provided you comply with the provisions of the Act and the following conditions of use:

- Any use you make of these documents or images must be for research or private study purposes only, and you may not make them available to any other person.
- Authors control the copyright of their thesis. You will recognise the author's right to be identified as the author of the thesis, and due acknowledgement will be made to the author where appropriate.
- You will obtain the author's permission before publishing any material from the thesis.

**The Preparation of Fluorescent Fingerprinting Powders  
using 8-Hydroxyquinoline Compounds and Magnetite**

A thesis  
submitted in partial fulfilment  
of the requirements for the degree  
of  
**Master of Science in Chemistry**  
at  
**The University of Waikato**

by  
**Benjamin Ross O'Shea**



THE UNIVERSITY OF  
**WAIKATO**  
*Te Whare Wānanga o Waikato*

2018

## Abstract

Fluorescent fingerprinting powders were prepared by using rotary evaporation to coat magnetite powder with varying amounts of either tris(8-hydroxyquinolino)aluminium ( $\text{Alq}_3$ ), tris(8-hydroxyquinolino)gallium ( $\text{Gaq}_3$ ), bis(8-hydroxyquinolino)magnesium ( $\text{Mgq}_2$ ) or bis(8-hydroxyquinolino)zinc ( $\text{Znq}_2$ ). The performance of each fingerprinting powder was tested on various surfaces under visible light and under UV excitation. The efficacy of powder application using a magnetic brush was compared to that of standard brushes. The effects of varying the particle sizes of the fingerprinting powders made with  $\text{Alq}_3$  and  $\text{Znq}_2$  were explored. The stability of each fluorescent compound under standard conditions was tested.

The synthesis of sodium tetrakis(8-hydroxyquinolino)boron ( $\text{NaBq}_4$ ) was attempted twice, but failed both times. The product acquired was suspected to be  $\text{Na}_4(\text{C}_9\text{H}_6\text{NO})_4(\text{H}_2\text{O})_8$  ( $\text{Na}_4\text{q}_4(\text{H}_2\text{O})_8$ ) instead. Crystals of  $\text{Na}_4\text{q}_4(\text{H}_2\text{O})_8$  were prepared using a modified literature method. The  $\text{Na}_4\text{q}_4(\text{H}_2\text{O})_8$  crystals and the products of the attempted syntheses were characterised by powder X-ray crystal diffraction, inductively coupled plasma mass spectrometry, electrospray ionisation mass spectrometry, nuclear magnetic resonance spectroscopy, UV-Vis absorption, and melting point measurements. Fingerprint powders were prepared using the products of the attempted  $\text{NaBq}_4$  syntheses and tested in the same manner as the  $\text{Alq}_3$ ,  $\text{Gaq}_3$ ,  $\text{Znq}_2$ , and  $\text{Mgq}_2$  fingerprint powders.

## Acknowledgements

I would like to thank Bill Henderson for being a fantastic supervisor and always being in a pleasant mood. Your feedback has been absolutely invaluable and your enthusiasm really helped to motivate me throughout this journey.

The staff at the University of Waikato have been extremely accommodating. There have been far too many people who have assisted me to list here, but John, Jenny, Annie, Karla, and Tom in particular deserve a mention for helping me hunt down various chemicals or pieces of equipment. Thank you to Graham Saunders for solving the structures of the crystals I grew for this thesis and to Helen for running the powder X-ray diffraction experiments.

I'd like to give a big thanks to my friends at the University for all the great times we've had. Thank you to Hayden for sharing your vast technical expertise. A special thanks to my friend James for sending the magnetic brush all the way from the USA.

Finally, I'd like to thank my family for always supporting me in this endeavour.

---

## Table of Contents

|  |          |
|--|----------|
| Title .....  | i        |
| Abstract.....  | ii       |
| Acknowledgements.....  | iii      |
| Table of Contents.....   | iv       |
| List of Figures .....  | vii      |
| List of Tables.....  | vii      |
| List of Abbreviations.....   | x        |
| <b>Chapter One: A Brief Review of Fingerprinting and Fluorescence.....</b> | <b>1</b> |
| 1.1 The Chemistry behind Fingerprint Analysis .....                        | 1        |
| 1.1.1 Introduction.....  | 1        |
| 1.1.2 Ninhydrin .....  | 3        |
| 1.1.3 Cyanoacrylate .....  | 5        |
| 1.1.4 Silver Nitrate.....  | 6        |
| 1.1.5 Gun Blue .....   | 6        |
| 1.1.6 Iodine.....  | 7        |
| 1.1.7 Oil Red O.....   | 8        |
| 1.1.8 Physical Developer.....  | 9        |
| 1.1.9 Small Particle Reagents .....  | 10       |
| 1.1.10 Vacuum Metal Deposition.....  | 10       |
| 1.1.11 Dusting Powders .....   | 12       |
| 1.2 Fluorescent Methods .....  | 13       |
| 1.2.1 Principles of Fluorescence .....                                     | 13       |
| 1.2.2 Fluorescent Powders.....   | 13       |
| 1.2.3 Fluorescent Colloidal Solutions .....                                | 15       |
| 1.2.4 Quantum Dots .....   | 15       |
| 1.2.5 Other Applications of Fluorescent Compounds .....                    | 16       |
| 1.2.6 Alq <sub>3</sub> .....   | 22       |
| 1.2.7 Derivatives of Alq <sub>3</sub> .....                                | 24       |
| 1.2.8 Analogues of Alq <sub>3</sub> .....                                  | 26       |

---

|  |           |
|--|-----------|
| 1.3 Conclusion.....  | 27        |
| 1.4 Scope of this Thesis .....   | 28        |
| 1.5 References .....   | 28        |
| <b>Chapter Two: Preparation of Fluorescent Magnetite-based Fingerprinting Powders.....</b>   | <b>35</b> |
| 2.1 Introduction.....  | 35        |
| 2.2 Experimental.....  | 37        |
| 2.2.1 Materials.....   | 37        |
| 2.2.2 Synthesis of Alq <sub>3</sub> .....  | 38        |
| 2.2.3 Synthesis of Gaq <sub>3</sub> .....  | 38        |
| 2.2.4 Synthesis of Znq <sub>2</sub> .....  | 39        |
| 2.2.5 Synthesis of Mgq <sub>2</sub> .....  | 39        |
| 2.2.6 Preparation of Fluorescent Fingerprint Powders .....   | 40        |
| 2.2.7 Application Method.....  | 41        |
| 2.2.8 Atmospheric Reactivity Tests .....   | 42        |
| 2.2.9 Assessment of Powders .....  | 42        |
| 2.3 Results.....   | 43        |
| 2.3.1 Syntheses.....   | 43        |
| 2.3.2 Fingerprint Tests .....  | 43        |
| 2.3.3 Effects of Fluorescent Component .....   | 45        |
| 2.3.4 Atmospheric Reactivity .....   | 48        |
| 2.3.5 Effects of Test Surface .....  | 50        |
| 2.3.6 Effects of Ratio .....   | 51        |
| 2.3.7 Effects of Application Method.....   | 52        |
| 2.3.8 Effects of Particle Size.....  | 53        |
| 2.4 Discussion .....   | 56        |
| 2.5 Conclusion.....  | 59        |
| 2.6 References .....   | 59        |
| <b>Chapter Three: Attempted Synthesis of Sodium Tetra(8-Hydroxyquinolato)Boron (NaBq<sub>4</sub>) and Preparation of Fluorescent Fingerprinting Powders using 8-Hydroxyquinoline Salts .....</b> | <b>62</b> |
| 3.1 Introduction.....  | 62        |
| 3.2 Experimental.....  | 64        |
| 3.2.1 Materials.....   | 64        |

---

|  |           |
|--|-----------|
| 3.2.2 Synthesis of NaBq <sub>4</sub> .....   | 64        |
| 3.2.3 Synthesis of Na <sub>4</sub> q <sub>4</sub> (H <sub>2</sub> O) <sub>8</sub> Crystals.....  | 65        |
| 3.2.4 Preparation of Fluorescent Fingerprinting Powders .....  | 66        |
| 3.2.5 Application Method.....  | 66        |
| 3.2.6 Assessment of Powders .....  | 66        |
| 3.2.7 Inductively Coupled Plasma Mass Spectrometry (ICP-MS)<br>Sample Preparation.....   | 67        |
| 3.2.8 Electrospray Ionisation Mass Spectrometry (ESI-MS)<br>Experiments. ....  | 67        |
| 3.2.9 Nuclear Magnetic Resonance (NMR) Spectroscopy Experiments<br>.....   | 68        |
| 3.2.10 UV-Vis Sample Preparation.....  | 69        |
| 3.2.11 XRD Experiments .....   | 69        |
| 3.3 Results of Characterisation Experiments.....   | 70        |
| 3.3.1 Physical Properties.....   | 70        |
| 3.3.2 Melting Point Measurements .....   | 71        |
| 3.3.3 Analysis by ICP-MS.....  | 73        |
| 3.3.4 Characterisation by ESI-MS .....   | 74        |
| 3.3.5 Characterisation by NMR .....  | 77        |
| 3.3.6 UV-Vis Absorbance Experiments .....  | 82        |
| 3.3.7 XRD Results.....   | 84        |
| 3.4 Characterisation Discussion .....  | 85        |
| 3.5 Fingerprinting Powder Performance .....  | 87        |
| 3.5.1 Effects of Powder Formulation .....  | 88        |
| 3.5.2 Effects of Test Surface .....  | 88        |
| 3.5.3 Effects of Application Method.....   | 90        |
| 3.6 Conclusion.....  | 91        |
| 3.7 References .....   | 92        |
| <b>Chapter Four: Concluding Remarks .....</b>  | <b>95</b> |
| <b>Appendix I: <sup>13</sup>C NMR Spectra of Substance A, Substance B,<br/>Na<sub>4</sub>q<sub>4</sub>(H<sub>2</sub>O)<sub>8</sub>, and 8-Hydroxyquinoline .....</b> | <b>97</b> |
| <b>Appendix II: Na<sub>4</sub>q<sub>4</sub>(H<sub>2</sub>O)<sub>8</sub> Crystal Data (DAMHOQ01) .....</b>  | <b>98</b> |
| <b>Appendix III: Crystal Structure of Na<sub>4</sub>q<sub>4</sub>(H<sub>2</sub>O)<sub>8</sub> (DAMHOQ01).....</b>  | <b>99</b> |

## List of Figures

|   |    |
|---|----|
| <b>Figure 1.1:</b> Various levels of magnification of human volar pads (a to c) and a histological cross section (d). .....   | 1  |
| <b>Figure 1.2:</b> Reaction of ninhydrin with an $\alpha$ -amino acid to form Ruhemann's Purple. ....   | 4  |
| <b>Figure 1.3:</b> 1,8-Diazafluoren-9-one .....   | 5  |
| <b>Figure 1.4:</b> Diagram showing the polymerisation of cyanoacrylate. ....  | 5  |
| <b>Figure 1.5:</b> Iodine print fixed with brucine. ....  | 8  |
| <b>Figure 1.6:</b> Oil Red O .....  | 8  |
| <b>Figure 1.7:</b> Oil Red O stained print.....   | 9  |
| <b>Figure 1.8:</b> Diagram of vacuum metal deposition adapted from Newton. ....   | 11 |
| <b>Figure 1.9:</b> Optimal gold deposition for VMD (left) compared to excess gold deposition (right). ....  | 11 |
| <b>Figure 1.10:</b> Colour transition of fingerprint visualised with a PDA/magnetite powder as it is exposed to UV irradiation and heating. ...   | 14 |
| <b>Figure 1.11:</b> Fingerprint visualised with quantum dots modified with N-acetylcysteine. Level two structures have been labelled. The small white circles indicate level three structures. .... | 16 |
| <b>Figure 1.12:</b> Diagram of a fluorescent rhenium complex with highly lipophilic groups used to image cytoplasm.....   | 18 |
| <b>Figure 1.13:</b> $[\text{Ru}(\text{bpy})_3]^{2+}$ ion .....  | 19 |
| <b>Figure 1.14:</b> $\text{Eu}(\text{tta})_3$ .....   | 20 |
| <b>Figure 1.15:</b> Diagram of a magnetite nanoparticle functionalised with a $\text{Tb}^{3+}$ complex.....   | 21 |
| <b>Figure 1.16:</b> Sample of $\text{Alq}_3$ under UV excitation. ....  | 22 |
| <b>Figure 1.17:</b> Diagram of $\text{Alq}_3$ modified with an electron withdrawing group. ....   | 25 |
| <b>Figure 1.18:</b> Diagram of $\text{Alq}_3$ modified with an electron donating group. ....  | 25 |
| <b>Figure 1.19:</b> Tris(4-morpholinyl-8-hydroxyquinolinato)aluminium.....  | 26 |
| <b>Figure 1.20:</b> $\text{Znq}_2$ under UV excitation. ....  | 27 |

|  |    |
|--|----|
| <b>Figure 2.1:</b> Fingerprint under UV light visualised by 20% MgM applied via zephyr brush. Note the large amount of background staining. ....   | 45 |
| <b>Figure 2.2:</b> Fingerprint under UV light visualised by 20% GM applied via zephyr brush. ....  | 46 |
| <b>Figure 2.3:</b> Fingerprints under visible light (top) and UV light (bottom) visualised by 20% AM applied via zephyr brush. ....  | 47 |
| <b>Figure 2.4:</b> Fingerprints under UV light (left) and visible light (right) visualised by 10% GM applied via magnetic brush. ....  | 47 |
| <b>Figure 2.5:</b> 500x magnification of a fingerprint visualised by 20% GM applied via magnetic brush. The farrow of the fingerprint is in focus, while the ridges are out of focus due to the narrow depth of field. ....  | 48 |
| <b>Figure 2.6:</b> Fingerprints on a plastic OHP sheet under UV light visualised by 20% AM, 10% AM, 20% ZM, and 10% ZM applied via zephyr brush..  | 51 |
| <b>Figure 2.7:</b> Fingerprints under UV light visualised by 10% GM applied via magnetic brush. Background staining made the prints very difficult to resolve. ....  | 52 |
| <b>Figure 2.8:</b> Fingerprint under UV light visualised by 20% GM applied via magnetic brush. Note the damage towards the left of the fingerprint caused by the magnetic brush.. ....   | 53 |
| <b>Figure 2.9:</b> Fingerprints on cans under UV light visualised by 20% AM <65 $\mu\text{m}$ (a), 20% AM 65-125 $\mu\text{m}$ (b), and 20% AM >125 $\mu\text{m}$ (c) powders applied via zephyr brush. ....   | 54 |
| <b>Figure 2.10:</b> Close up of a fingerprint under UV light visualised by 20% AM >125 $\mu\text{m}$ applied via zephyr brush. The black circle on the image highlights some of the level three structures visible (level three fingerprint structures are described in section 1.2.4). .... | 55 |
| <b>Figure 2.11:</b> Fingerprints under UV light visualised by 10% ZM <65 $\mu\text{m}$ (a), 10% ZM 65-125 $\mu\text{m}$ (b), and 10% ZM >125 $\mu\text{m}$ (c) applied via zephyr brush. ....  | 56 |
| <b>Figure 3.1:</b> Structure of $\text{Na}_4\text{q}_4(\text{H}_2\text{O})_8$ . The elements are colour coded white, grey, blue, red and purple for hydrogen, carbon, nitrogen, oxygen, and sodium, respectively. ....   | 63 |

|   |    |
|---|----|
| <b>Figure 3.2:</b> $m/z$ 357 peak in the positive ion ESI mass spectrum of substance <b>A</b> . Note that the doubling of peaks was an artefact caused by the instrument. ....  | 75 |
| <b>Figure 3.3:</b> Main peaks of the negative ion ESI mass spectrum of substance <b>A</b> . ....  | 76 |
| <b>Figure 3.4:</b> $m/z$ 168 peak in the positive ion ESI mass spectrum of $\text{Na}_4\text{q}_4(\text{H}_2\text{O})_8$ (90/30 V). ....  | 77 |
| <b>Figure 3.5:</b> $^1\text{H}$ NMR spectra (6.5 ppm to 9 ppm) of substance <b>A</b> , substance <b>B</b> , $\text{Na}_4\text{q}_4(\text{H}_2\text{O})_8$ and 8-hydroxyquinoline. ....                                    | 79 |
| <b>Figure 3.6:</b> $^1\text{H}$ NMR spectrum of 8-hydroxyquinoline. The peak assignments are in agreement with literature values. ....  | 80 |
| <b>Figure 3.7:</b> Partial $^1\text{H}$ NMR spectra of $\text{Na}_4\text{q}_4(\text{H}_2\text{O})_8$ (top) and substance <b>A</b> (bottom). ....  | 81 |
| <b>Figure 3.8:</b> $\delta$ 8.61 peak in the $^1\text{H}$ NMR spectrum of $\text{Na}_4\text{q}_4(\text{H}_2\text{O})_8$ (top) and $\delta$ 8.64 peak in the $^1\text{H}$ NMR spectrum of substance <b>A</b> (bottom)..... | 82 |
| <b>Figure 3.9:</b> Graph showing the UV-Vis absorbances of substance <b>A</b> , substance <b>B</b> , and $\text{Na}_4\text{q}_4(\text{H}_2\text{O})_8$ .....  | 83 |
| <b>Figure 3.10:</b> Powder diffraction patterns of substance <b>A</b> (solid) and substance <b>B</b> (dashed). ....   | 84 |
| <b>Figure 3.11:</b> Powder diffraction pattern of $\text{Na}_4\text{q}_4(\text{H}_2\text{O})_8$ . ....  | 85 |
| <b>Figure 3.12:</b> Fingerprint visualised by 20% BM applied via zephyr brush under UV light. ....  | 89 |
| <b>Figure 3.13:</b> Fingerprint visualised by 10% BM2 applied via zephyr brush under UV light. ....   | 90 |
| <b>Figure 3.14:</b> Attempted visualisation of fingerprint by 20% BM applied via magnetic brush under UV light. ....  | 91 |

## List of Tables

|   |    |
|---|----|
| <b>Table 2.1:</b> Reagents and Solvents .....                                 | 37 |
| <b>Table 2.2:</b> Equipment .....   | 37 |
| <b>Table 2.3:</b> Test Surfaces .....   | 37 |
| <b>Table 2.4:</b> List of Powder Formulations .....                           | 41 |
| <b>Table 2.5:</b> Quality Grades .....  | 42 |
| <b>Table 2.6:</b> Conditions of Fingerprinting Tests .....                    | 44 |
| <b>Table 3.1:</b> Chemicals.....  | 64 |
| <b>Table 3.2:</b> Equipment .....   | 64 |
| <b>Table 3.3:</b> Powder Diffractometer Settings.....                         | 70 |
| <b>Table 3.4:</b> Transition temperatures measured by the Büchi apparatus ... | 72 |
| <b>Table 3.5:</b> Conditions of Fingerprinting Tests .....                    | 87 |

## List of Abbreviations

DFO – 1,8-Diazafluoren-9-one

UV – Ultra-violet

UV-Vis – Ultra-violet visible

Redox – Reduction-oxidation

VMD – Vacuum metal deposition

LUMO – Lowest unoccupied molecular orbital

HOMO – Highest occupied molecular orbital

PDA – Polydiacetylene

Eu(tta)<sub>3</sub> – Tris(thenoyltrifluoroacetato)europium

CRT – Cathode ray tube

LCD – Liquid crystal display

OLED – Organic light emitting diode

Alq<sub>3</sub> – Tris(8-hydroxyquinolino)aluminium

Gaq<sub>3</sub> – Tris(8-hydroxyquinolino)gallium

Znq<sub>2</sub> – Bis(8-hydroxyquinolino)zinc

Mgq<sub>2</sub> – Bis(8-hydroxyquinolino)magnesium

AM – Alq<sub>3</sub>/magnetite

GM – Gaq<sub>3</sub>/magnetite

MgM – Mgq<sub>2</sub>/magnetite

ZM – Znq<sub>2</sub>/magnetite

OHP – Overhead projector

DMSO – Dimethyl sulfoxide

d6-DMSO – Deuterated dimethyl sulfoxide

NaBq<sub>4</sub> – Na[B(C<sub>9</sub>H<sub>6</sub>NO)<sub>4</sub>]

Na<sub>4</sub>q<sub>4</sub>(H<sub>2</sub>O)<sub>8</sub> – Na<sub>4</sub>(C<sub>9</sub>H<sub>6</sub>NO)<sub>4</sub>(H<sub>2</sub>O)<sub>8</sub>

Hq – 8-Hydroxyquinoline

q – Deprotonated 8-hydroxyquinoline

δ – Chemical shift

s – Singlet

d – Doublet

dd – Doublet of doublets

t – Triplet

m – Multiplet

br – Broad

J – Coupling constant

CCDC – Cambridge Crystallographic Data Centre

## Chapter One: A Brief Review of Fingerprinting and Fluorescence

### 1.1 The Chemistry behind Fingerprint Analysis

#### 1.1.1 Introduction

Knowledge of fingerprints extends back to at least 300 BC, as they were used by the Chinese to signify the ownership of property. However, it was not until the late 1800s that scientists began to investigate fingerprints for solving crime. In the early 1900s, systems for matching fingerprints to suspects were in place around the world.

The patterns of the ridges and furrows of human volar pads (see Fig. 1.1) are developed in the womb. They remain the same unless permanently damaged and are unique to the individual. This makes a fingerprint a highly useful identifier.

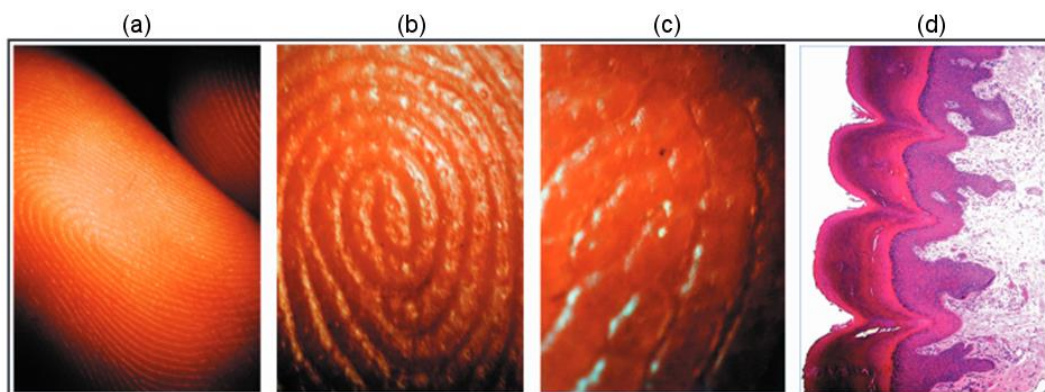


**Figure 1.1:** Various levels of magnification of human volar pads (a to c) and a histological cross section (d).<sup>[1]</sup>

There are three kinds of fingerprint commonly found at crime scenes: plastic, patent, and latent. Plastic prints form when the finger pushes into something soft and leaves an impression; materials such as fresh paint and putties allow for plastic prints. Patent prints are produced when a visible foreign substance coating the finger is deposited on to a surface, for example, blood on a door handle. Latent prints are similar to patent prints but instead of foreign material, they are formed by skin secretions and are largely invisible without development. Sweat and sebum are the two main secretions responsible for latent prints. Sweat contains many water soluble compounds that are often targeted by fingerprint reagents to produce coloured species. Sebum is made of non-water-soluble lipids which allow for the visualisation of prints that have been wet.<sup>[2]</sup> Latent prints are the most common type of print used to solve crime.

The reliability of fingerprints as evidence for linking a suspect to a location or piece of evidence has led to the widespread use of forensic fingerprinting and created demand for the development of new techniques for visualising prints. The Federal Bureau of Investigation alone has collected at least 238 million prints in its lifetime.<sup>[3]</sup>

There have been many different methods developed for the visualisation of prints, but they can generally be placed into one of two categories, physical or chemical. Physical methods rely on a physical affinity for the print so that the reagent is more likely to adhere to the print rather than the surface the print is deposited on. Chemical methods often

target species present in fingerprints, reacting with them to form a visible compound.

Since the conditions for each print can vary so widely, an extensive range of reagents has been developed to suit every situation. The following literature review will cover some of the physical and chemical methods used to visualise latent fingerprints. The principles of fluorescence are also reviewed, as several techniques rely on it to visualise fingerprints. Additionally, the versatility of fluorescent compounds is explored through various examples of applications that utilise them.

### *1.1.2 Ninhydrin*

Ninhydrin is a widely used fingerprinting reagent that was patented in 1955.<sup>[4]</sup> It visualises fingerprints by reacting with primary amines present in human sweat to form a pigment known as Ruhemann's Purple (see Fig. 1.2). Secondary amines also react with ninhydrin, but instead of forming Ruhemann's Purple, they form a yellow iminium salt. Common practice for using ninhydrin to visualise prints on paper involves dissolving ninhydrin in a volatile solvent, such as ethanol, and applying it as a spray. Heating the article in an oven may be desirable to speed the reaction.<sup>[5]</sup>

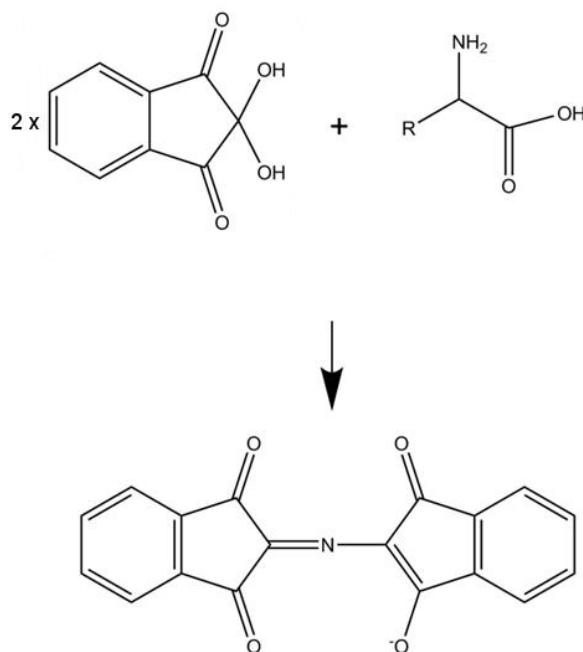


**Figure 1.2:** Reaction of ninhydrin with an  $\alpha$ -amino acid to form Ruhemann's Purple.

Addition of zinc chloride enhances the detection of Ruhemann's Purple by improving its ability to fluoresce. This is achieved by the formation of a Ruhemann's Purple/ $\text{Zn}^{2+}$  complex, as the zinc cation forces the ring systems into a coplanar conformation. The coplanar conformation increases conjugation, allowing the complex to fluoresce when subjected to laser excitation.<sup>[6]</sup>

1,8-Diazafluoren-9-one (DFO) (see Fig. 1.3) was first synthesised in 1950, but was not widely used for visualising fingerprints until 1989. DFO reacts with amines in a similar manner to ninhydrin, giving a green-yellow fluorescent complex. DFO could be considered to be superior to ninhydrin as it does not require the formation of a metal complex to exhibit UV activity.<sup>[7]</sup>

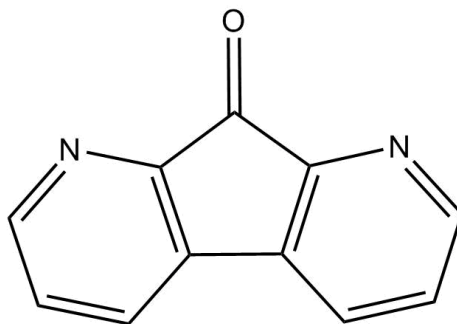


**Figure 1.3:** 1,8-Diazafluoren-9-one

### 1.1.3 Cyanoacrylate

Cyanoacrylate, more commonly known as ‘superglue’, has been used for the detection of latent fingerprints since the 1980s. Cyanoacrylate is applied as a heated vapour and visualises fingerprints by forming a light coloured polymer on contact with the fingerprint (see Fig. 1.4). The mechanism of polymerisation is complex and not particularly well understood, but it is suggested that the polymerisation is catalysed by the  $\text{OH}^-$  present in the print.<sup>[8]</sup>

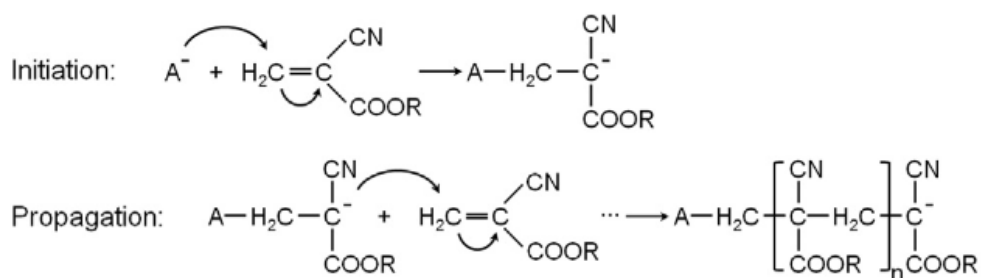


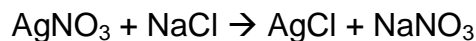
**Figure 1.4:** Diagram showing the polymerisation of cyanoacrylate.<sup>[9]</sup>

Cyanoacrylate is most effective for visualising latent prints on non-porous surfaces such as plastic, glass, or metal. The major advantage of using cyanoacrylate is that it can be used to visualise prints for an entire

crime scene in one to two hours. This is achieved by sealing the crime scene and using a compressor to pump cyanoacrylate vapour into it. Fans set up inside the scene may be used to better circulate the vapours. The visualisation progress can be monitored by placing foil with exemplar prints on them at locations visible from outside the sealed crime scene. After the development of the fingerprints, the crime scene must be thoroughly ventilated as cyanoacrylate vapours are toxic and flammable.<sup>[8]</sup>

#### 1.1.4 Silver Nitrate

Silver nitrate is a relatively old method of fingerprint development, as it has been in use since the 1930s. Silver nitrate is applied in aqueous solution as a spray and works by reacting with the sodium chloride present in the fingerprint, allowing it to be used on prints that are months old:



It is usually necessary to develop the print further by exposing it to strong light, as this improves the visibility of the print. This results in the deposition of silver metal and evolution of chlorine gas:



The resulting print is usually of high quality, but the method is time consuming and destructive when applied to documents.<sup>[10]</sup>

#### 1.1.5 Gun Blue

'Gun blue' solutions offer a unique and very specific method of visualising prints. Gun blue is a mixture of copper sulfate and selenous acid in aqueous solution. As the name implies, it is used for detecting

prints on brass shell casings. The common procedure for its use involves immersing the casing in the solution, which leads to copper selenide deposits forming on the brass. However, the lipids present in the fingerprint do not react with gun blue, so the outlines of any prints are clearly shown as the rest of the casing is covered in the blue film made of copper selenide.<sup>[11]</sup>

#### *1.1.6 Iodine*

Iodine fuming has been used since the late 1800s to develop fingerprints. Common practice involves gently heating iodine crystals in a sealed vessel until they sublime. The fumes adsorb to the lipids, such as sebum, in the print. The resulting visualised fingerprint is a yellow-brown colour. Iodine fuming was originally thought to be a chemical method, but it has also been suggested to be a physical interaction, as the iodine adsorbs to the print.<sup>[11]</sup>

Treatment with iodine is a cheap and simple method that may be used on various porous and non-porous surfaces, but unfortunately fingerprints visualised by iodine do not remain so for very long, as the iodine will eventually diffuse out. In order to prevent the prints from becoming invisible again, various reagents can be used to 'fix' the prints. Starch, water, 7,8-benzoflavone, and more recently, brucine solutions, have been used as fixing reagents for iodine prints (see Fig. 1.5). They may be applied by fuming or dipping, depending on the surface the fingerprint is adhered to. Each fixing reagent uses a different mechanism, but the basic principle is to slow the sublimation of the iodine.<sup>[11]</sup>



**Figure 1.5:** Iodine print fixed with brucine.<sup>[11]</sup>

### 1.1.7 Oil Red O

Oil Red O (see Fig 1.6), aka Sudan Red 5B, is a lysochrome (a fat soluble dye) with a variety of uses in industry, such as in fireworks, leather tanning, and biological staining. It has only recently been used for forensic purposes.

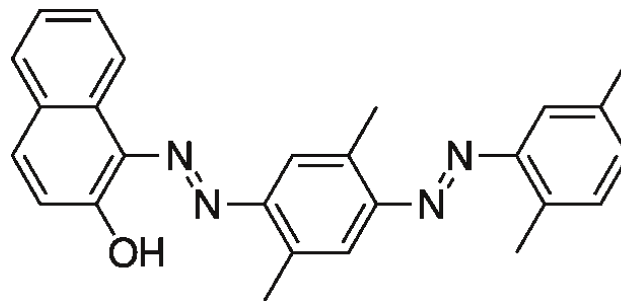


**Figure 1.6:** Oil Red O<sup>[12]</sup>

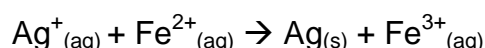
Oil Red O is typically used on porous surfaces, such as cardboard and paper, as a solution with sodium hydroxide in methanol. Oil Red O readily concentrates in the lipids of the fingerprint, giving them a bright red stain, while dyeing the surrounding surface a light pink (see Fig. 1.7). This mode of action means it works even when the material is wet.<sup>[12]</sup>



**Figure 1.7:** Oil Red O stained print.<sup>[12]</sup>

### 1.1.8 Physical Developer

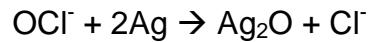
A mixture of  $\text{Ag}^+$  and  $\text{Fe}^{2+}$  can be used to develop prints through simple reduction-oxidation chemistry. This is known as physical developer. Instead of targeting water soluble components, such as  $\text{Cl}^-$ , physical developer targets the insoluble components of the print, as it relies on the silver ions being reduced to silver metal by the iron ions, which oxidise to  $\text{Fe}^{3+}$ :



This allows for the development of latent fingerprints on wet surfaces.<sup>[13]</sup>

The redox reaction of  $\text{Ag}^+$  and  $\text{Fe}^{2+}$  is reversible, so additional species are added to the physical developer solution to slow the rate of oxidation of the silver metal. Citric acid is added to manipulate the equilibrium. It does this by complexing with  $\text{Fe}^{3+}$ , effectively excluding it from the equilibrium and promoting the oxidation of  $\text{Fe}^{2+}$ . Citric acid also lowers the pH, which is desirable because superior results are obtained under slightly acidic conditions. Physical developer works best when the silver particles are finely divided, so *n*-dodecylammonium acetate is added

to keep the silver particles separate. It achieves this by attaching to the particles and imparting a positive charge, causing the particles to repel each other. This is known as peptisation.<sup>[13]</sup> Sodium hypochlorite improves the appearance of developed prints by oxidising the silver to silver oxide, which has a much darker colour:



This process is called 'bleach toning'. The background surface is made lighter by the bleaching process, further increasing contrast with the dark silver oxide.<sup>[13]</sup> The use of physical developer followed by bleach toning produces high quality prints, but is a rather involved process.

#### *1.1.9 Small Particle Reagents*

Small particle reagents used to visualise fingerprints commonly utilise metal salts mixed with a surfactant. The hydrophilic end of the surfactant binds to the salt, while the hydrophobic end of the surfactant molecule is attracted to the lipids present in the print. This results in the coloured complex adhering to the print even in wet conditions. The metal compound is most commonly molybdenum sulfide, but compounds such as titanium dioxide, zinc carbonate, and magnetite are also used in small particle reagents.<sup>[14]</sup> The reagent is typically sprayed on to the surface, with excess being washed off, leaving behind the visualised print.

#### *1.1.10 Vacuum Metal Deposition*

Vacuum metal deposition (VMD) is a fairly modern technique for developing fingerprints. It offers excellent sensitivity, even for old prints,

but has issues with reliability, complexity, and high cost. The process of VMD involves depositing evaporated gold on to the surface to be visualised, followed by a coating of zinc applied in the same manner. The gold will uniformly coat the entire surface (including penetrating through the eccrine secretions of the fingerprint as shown in Fig. 1.8), but the zinc will only deposit on the gold, resulting in a grey surface with gold fingerprints. VMD may run into issues as the zinc can sometimes deposit on the prints or too much gold may coat the surface, decreasing the visibility of the prints (see Fig. 1.9).<sup>[15][16]</sup>

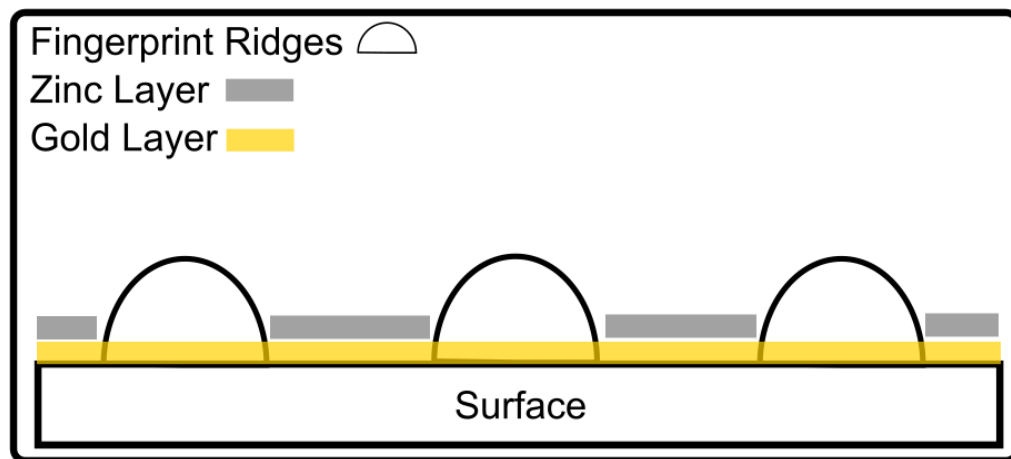


**Figure 1.8:** Diagram of vacuum metal deposition adapted from Newton.<sup>[3]</sup>

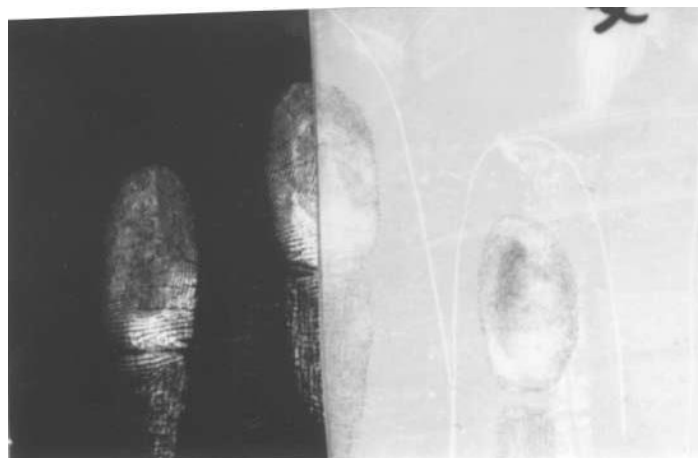


**Figure 1.9:** Optimal gold deposition for VMD (left) compared to excess gold deposition (right).<sup>[15]</sup>

### 1.1.11 Dusting Powders

Dusting powders are a rapid and simple method of developing fingerprints. The use of dusting powders is a physical method, as the particles mechanically adhere to the print. Dusting powders are applied using brushes with bristles made of nylon, camel hair, fibreglass, or another sufficiently fine material. Magnetic powders may be applied with magnetic brushes. These brushes lack bristles; instead using a magnet attached to a plunger in a plastic sheath to hold and release the powder as necessary. Magnetic brushes can reduce the amount of excess powder applied by waving the 'empty' brush over the print again to pick up any powder not adhered to the print. Magnetic brushes may also help preserve print details as they may apply powder more gently than fibre brushes.<sup>[17]</sup>

The compositions of dusting powders vary greatly to suit specific applications. Factors to consider when choosing a powder may include the porosity, colour, or magnetic properties of the surface. To fulfil these niches, powders may be made from materials such as polymers, dyes, metals, graphite, and more. Unlike some other methods, powder applications may be 'lifted' with tape so that the print may be taken away from the crime scene and filed appropriately.

While dusting powders may be faster than other methods, they have two main disadvantages when compared to some other methods. The first is that dusting powders require a relatively high amount of eccrine secretion to adhere; depending on the powder, this may be as much as 500 ng, compared to the 100-200 ng that most chemical methods require. Since components of a fingerprint may evaporate as they age, this leaves

less material for a dusting powder to attach to, resulting in reduced effectiveness for aged prints.<sup>[3]</sup>

## **1.2 Fluorescent Methods**

### *1.2.1 Principles of Fluorescence*

Luminescence occurs when a structure in an excited state emits light to return to equilibrium.<sup>[18]</sup> Fluorescence is a form of luminescence, characterised by the very short delay between excitation and emission, as well as ceasing almost immediately once excitation has stopped. UV (ultra-violet) radiation is a common type of excitation, which promotes an electron from the HOMO to the LUMO. The intensity of the fluorescence is relative to the intensity of the excitation source. The wavelength of the emission is dependent on the structure of the compound and it is always longer than the excitation wavelength. Fluorescence is more common in compounds that contain conjugated  $\pi$  systems that restrict vibrational relaxation and may be quenched by impurities, increases in temperature, or by increases in the strength of the intermolecular attractions.<sup>[19]</sup>

### *1.2.2 Fluorescent Powders*

Contrast between the powder and dusting surface is an important factor to consider when evaluating the performance of a dusting powder. The addition of fluorescent components greatly improves the contrast under UV light. The fluorescent compounds may not have desirable physical properties so they may be added in small amounts so as not to compromise adhesion. Aluminium nitride phosphors doped with lanthanide

ions have been shown<sup>[20]</sup> to give good contrast under UV excitation. However, fluorescent materials are often lightly coloured, which can make them difficult to detect when dusting large, lightly coloured surfaces.

Magnetite is a good bulk material to dope with fluorescent compounds because its dark colour provides strong contrast on light surfaces under visible light. Other attractive properties of magnetite include being cheap and magnetic, so it may be applied with a magnetic brush. Dark powders with fluorescent additives are available commercially.<sup>[21]</sup>

Polydiacetylenes (PDAs) are polymers that have photophysical properties which change based on stimuli, such as heat or UV irradiation. In a study by Lee *et al.*,<sup>[22]</sup> PDAs were mixed with magnetite nanoparticles to form dusting powders that change colour depending on treatment. Unlike conventional fluorescent powders, UV irradiation causes permanent colour changes in fingerprints treated with these PDA/magnetite powders. The colour may be altered again by heating, as shown in Fig. 1.10.<sup>[22]</sup> In addition to visible colour changes, this particular PDA/magnetite powder exhibits red fluorescence under UV light.

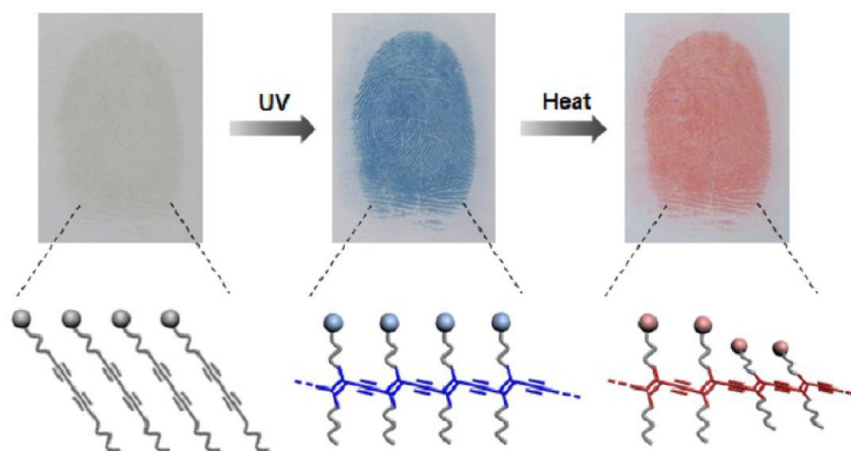


**Figure 1.10:** Colour transition of fingerprint visualised with a PDA/magnetite powder as it is exposed to UV irradiation and heating.<sup>[22]</sup>

### 1.2.3 Fluorescent Colloidal Solutions

An alternative method of applying fluorescent nanoparticles to latent prints is submersion in a colloidal solution. Fingerprints are lifted from the crime scene using tape, and developed in the colloidal solution within minutes, as the nanoparticles are immobilised on the fingerprint. Poly(p-phenylenevinylene) is an ideal candidate for colloidal solutions due to its low cost, low toxicity, and bright green fluorescence.<sup>[23]</sup>

### 1.2.4 Quantum Dots

Quantum dots are fluorescent particles that are only a few nanometres in diameter. Unlike most other fingerprint reagents, quantum dots are small enough to create pore maps. Pore maps are generated from the arrangement of pores in a fingerprint. The patterns of ridges and furrows that make up a fingerprint may be referred to as 'level two' structures, while pore maps are considered to be 'level three' structures, as they are of higher detail and require optical magnification to resolve. Individual pores do not always secrete sweat, so pore patterns from the same finger may differ to some degree. The variability of pore patterns means they should be used in conjunction with level two structures when matching fingerprints.<sup>[24]</sup>

Quantum dots visualise latent prints in the same manner as other fluorescent colloidal solutions; the difference is the degree of resolution possible.<sup>[25]</sup> In a study by Li *et al.*,<sup>[24]</sup> cadmium telluride quantum dots were functionalised with N-acetylcysteine ligands to increase their affinity for

fingerprints. The modified quantum dots fluoresced red under UV light and gave excellent resolution (see Fig. 1.11).

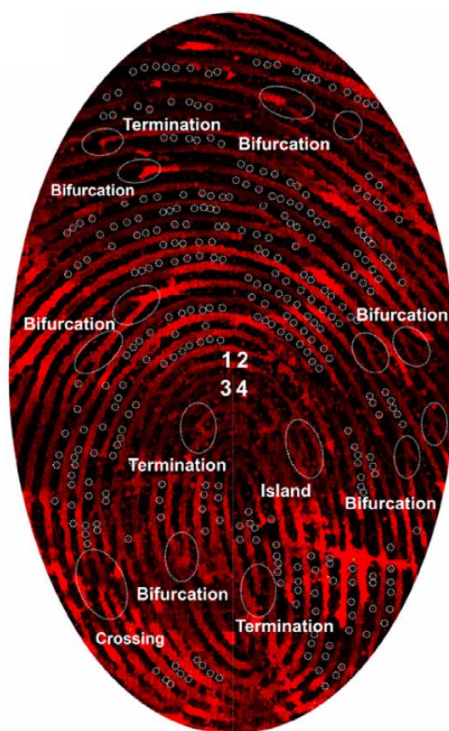


**Figure 1.11:** Fingerprint visualised with quantum dots modified with N-acetylcysteine. Level two structures have been labelled. The small white circles indicate level three structures.<sup>[24]</sup>

### 1.2.5 Other Applications of Fluorescent Compounds

Luminescence was first investigated in Italy during the 17<sup>th</sup> century, when barium sulfide synthesised from barium sulfate was discovered to glow after exposure to sunlight.<sup>[18]</sup> The term “fluorescence” was coined in 1852 by Sir George Stokes to describe the short-lived emission of yellow light by the mineral fluorspar when excited by blue light.<sup>[18]</sup> Since then, fluorescent compounds have been used in a variety of applications.

Fluorescent lamps operate by applying an electric current to mercury vapour, which causes it to emit UV radiation. The radiation is absorbed by the phosphor that coats the interior of the tube, which in turn fluoresces in the visible spectrum. The phosphor is commonly made from calcium halophosphate doped with manganese and antimony ions. The manganese and antimony ions fluoresce yellow and blue light, respectively, to give white light.<sup>[26]</sup>

Cell imaging involves the use of fluorescent organometallic compounds to improve contrast between biological systems.<sup>[27]</sup> These materials typically involve an aryl multidentate ligand, such as bipyridine or 4,4'-benzene-1,3-diyl-dipyridine, bonded to a platinum group metal atom. There are numerous environments that can be stained within an organism, each with their own conditions. In order to be taken up by a biological system, the fluorescent complex may need to be modified to exhibit an affinity for said system. In addition to solubility, the metal complexes may be altered for specific fluorescence characteristics or decreased toxicity.  $[\text{Ir}(\text{phenylpyrazole})_2(\text{dipyridoquinoxaline})]^{3+}$  is an example of a complex that can be used for nucleolar staining due to its compatible lipophilicity and electronic properties. The cytoplasm is another important component of the cell that requires lipophilic complexes to image (see Fig. 1.12).

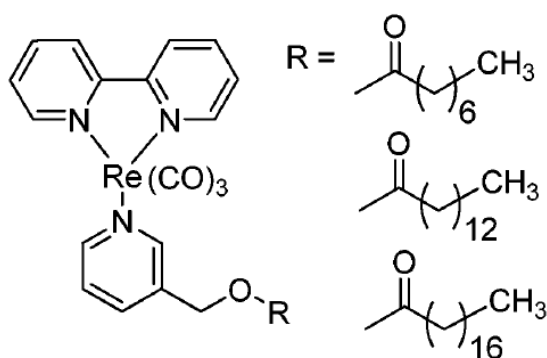


**Figure 1.12:** Diagram of a fluorescent rhenium complex with highly lipophilic groups used to image cytoplasm.<sup>[28]</sup>

Complexes that fluoresce at longer wavelengths are of particular interest for biological staining due to more effective tissue penetration. When exposed to UV light, some cell components emit light without the addition of a fluorescent complex; this is known as autofluorescence. These emissions are usually of a shorter wavelength, so metal complexes that emit red light provide good contrast.<sup>[28]</sup>

The fluorescence of metal complexes may change upon binding to organic molecules, as their electronic properties are altered. The change in fluorescence can be monitored and used to determine the concentration of important biological molecules. For example, 2,2'-dipicolylamine-zinc(II) derivatised with a fluorophore can be used as a chemical sensor for adenosine triphosphate.<sup>[29]</sup> 2,2'-Dipicolylamine can also be used to detect zinc and cadmium ions, as coordination to the ions will affect the molecule's photophysical properties.<sup>[28]</sup>

Fluorescent metal complexes may also be used as chemical sensors for intracellular oxygen. Ruda-Eberenz *et al.*<sup>[30]</sup> used tris(bipyridine)ruthenium ( $[\text{Ru}(\text{bpy})_3]^{2+}$ ) (see Fig. 1.13) for such a purpose.

The  $[\text{Ru}(\text{bpy})_3]^{2+}$  ions were immobilised on a zeolite support and submerged in an aqueous medium containing human monocytes. The fluorescence of  $[\text{Ru}(\text{bpy})_3]^{2+}$  is quenched by oxygen, so dissolved oxygen levels can be measured optically.

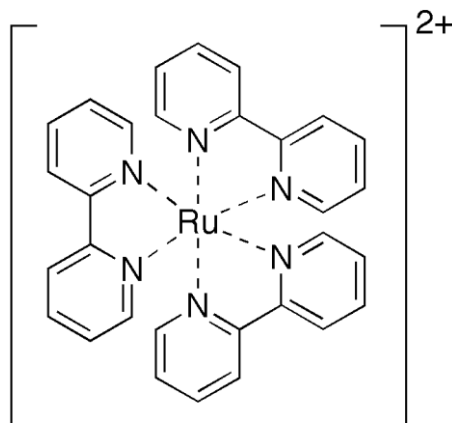


**Figure 1.13:**  $[\text{Ru}(\text{bpy})_3]^{2+}$  ion

Lanthanides are well known for their fluorescent  $\text{Ln}^{3+}$  ions. Although chemically quite similar, the fluorescence colours of  $\text{Ln}^{3+}$  ions vary widely. For example,  $\text{Tm}^{3+}$  emits blue light, while  $\text{Eu}^{3+}$  emissions are deep red.  $\text{Yb}^{3+}$ ,  $\text{Nd}^{3+}$ , and  $\text{Er}^{3+}$  are of particular interest for biological applications due to their near-infra-red fluorescence. Aromatic ligands with conjugated  $\pi$  systems, such as bipyridine, 8-hydroxyquinoline (Hq), and naphthalene, are sometimes called 'antenna' ligands. Antenna ligands are chromophores that affect the photophysical properties of  $\text{Ln}^{3+}$  complexes. In industry, antenna ligands are commonly used to tune fluorescence colour or improve efficiency.<sup>[31]</sup>

Tris(thenoyltrifluoroacetato)europium ( $\text{Eu}(\text{tta})_3$ ) is an example of a fluorescent lanthanide complex (see Fig. 1.14).

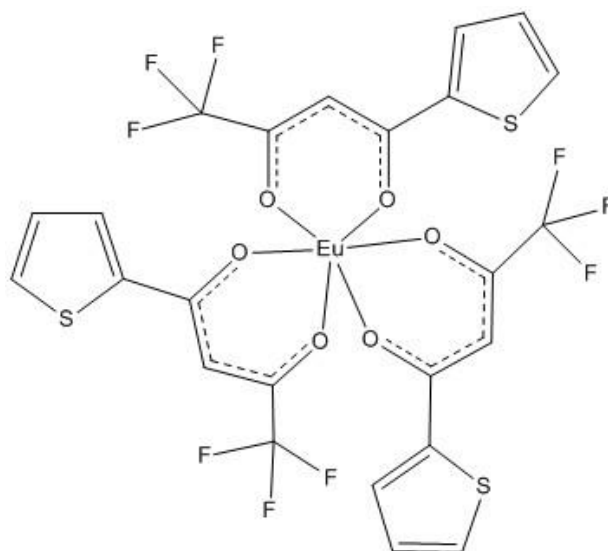


**Figure 1.14:**  $\text{Eu}(\text{tta})_3$

The fluorescence intensity of  $\text{Eu}(\text{tta})_3$  changes in response to temperature,<sup>[32]</sup> making it a good material to use as the fluorescent agent in temperature sensitive paints. Temperature sensitive paints are used in conjunction with high speed cameras to measure the temperature of systems that are difficult to measure by more conventional means. Temperature sensitive paints also offer improved resolution over other methods of measurement. In a study performed by Tsukamoto *et al.*,<sup>[33]</sup> temperature differences of  $\sim 0.2^\circ\text{C}$  could be detected every 0.2 ms, between positions  $39\ \mu\text{m}$  apart by temperature sensitive paints.

In a study by Wang *et al.*,<sup>[34]</sup> fluorescent activity was imparted to magnetite by functionalising its surface with a  $\text{Tb}^{3+}$  complex. In this case, the antenna ligand served to immobilise the  $\text{Tb}^{3+}$  ions on the magnetite nanoparticles as well as increase the solubility of the particles in aqueous media. The particles were also functionalised with folic acid ligands to increase their affinity for folate receptors (see Fig. 1.15).

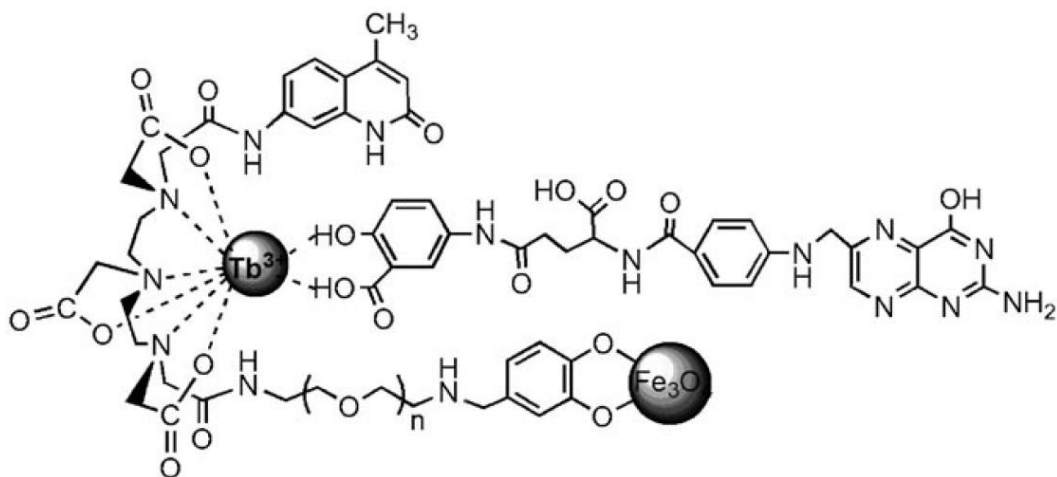


**Figure 1.15:** Diagram of a magnetite nanoparticle functionalised with a  $Tb^{3+}$  complex.<sup>[34]</sup>

Human cancer cells often have higher than normal folate receptors on their surface and will therefore have an increased uptake of the functionalised particles. When viewed under UV light, the cancer cells will glow brighter due to increased  $Tb^{3+}$  concentration.<sup>[34]</sup>

Cathode ray tube (CRT) televisions and computer monitors utilise europium based phosphors to provide red light for pixels.<sup>[35]</sup> These devices have since been phased out, as liquid crystal display (LCD) technology has developed. LCD screens make use of a zinc oxide, which is a fluorescent semiconductor that is used in a variety of optoelectronic devices.<sup>[18]</sup>

Just as CRT screens were superseded by LCD devices, organic light-emitting diode (OLED) displays are set to replace LCDs.<sup>[36]</sup> The competitive nature of the electronics industry means there has been a substantial amount of time and resources spent on improving OLEDs, with tris(8-hydroxyquinolino)aluminium ( $Alq_3$ ) being the most heavily

investigated compound in the field. There has also been much investigation into derivatives and analogues of Alq<sub>3</sub>, in hopes of maximising efficiency and performance. The following sections will examine Alq<sub>3</sub> more thoroughly as well as compare its fluorescence properties with those of its derivatives and analogues.

### 1.2.6 Alq<sub>3</sub>

Alq<sub>3</sub> consists of three deprotonated 8-hydroxyquinoline molecules (q) bonded as bidentate ligands to an aluminium(III) core. Alq<sub>3</sub> has several crystal phases that vary in appearance, but to the naked eye, they all resemble bright yellow powders. The melting point of Alq<sub>3</sub> varies with crystal phase. For example, the  $\alpha$ -phase melts at 395°C; note that Alq<sub>3</sub> decomposes above 430°C.<sup>[37]</sup> Under UV excitation, Alq<sub>3</sub> emits strongly in the green region around 500 nm (see Fig. 1.16), however this also varies with phase.<sup>[36][37]</sup>

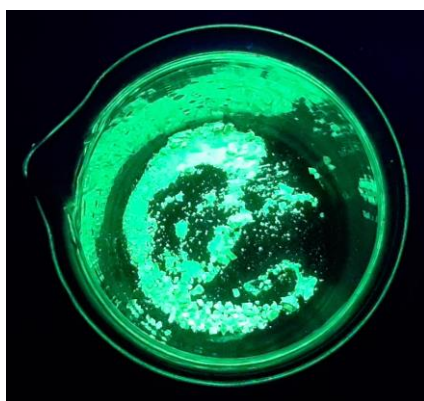


**Figure 1.16:** Sample of Alq<sub>3</sub> under UV excitation.

The fluorescence of Alq<sub>3</sub> involves promotion of an electron from the singlet state (spin quantum number = 0, “S<sub>0</sub>”) to the triplet state (spin

quantum number = 1, “S<sub>1</sub>”), followed by the relaxation from the triplet state back to the singlet state. Electrons may relax from the S<sub>1</sub> state to a third triplet state “T<sub>1</sub>” before returning to S<sub>0</sub>. The transition from T<sub>1</sub> to S<sub>0</sub> is forbidden, which leads to a long lifetime. The T<sub>1</sub>-S<sub>0</sub> transition is also incapable of relaxing via emission of a photon. When subjected to UV radiation for an excessive duration, an equilibrium system forms for the S<sub>1</sub>-T<sub>1</sub> and T<sub>1</sub>-S<sub>0</sub> transitions. This leads to an increase in the number of T<sub>1</sub> states and hence reduces the intensity of the fluorescence.<sup>[37]</sup>

Alq<sub>3</sub> loses its luminescent activity as it degrades within hours if left exposed to air and moisture. For this reason, it should be kept in an air-tight container and stored in the dark, as light exposure increases the rate of degradation.<sup>[38]</sup> Hydrolysis of Alq<sub>3</sub>, followed by oxidation of the ligand, generates a brown polymer that does not fluoresce. Other degradation products include [Alq<sub>2</sub>OH] and [(Alq<sub>2</sub>)<sub>2</sub>O]. These compounds may also form during synthesis of Alq<sub>3</sub> under basic conditions at elevated temperatures.<sup>[39]</sup> The reactivity of Alq<sub>3</sub> with the atmosphere is not an issue for visualising fingerprints, as they are photographed after visualisation. However, it may have an impact on the shelf-life of the reagent.

Alq<sub>3</sub> can be produced quickly and cheaply by adding 8-hydroxyquinoline and an aluminium(III) salt to a weakly acidic aqueous solution. Base is added dropwise while stirring to precipitate Alq<sub>3</sub>. The precipitate is retrieved by filtering and washing with distilled water. Analogues of Alq<sub>3</sub> may be prepared by substituting the aluminium salt for a salt of the desired metal.<sup>[36]</sup>

### 1.2.7 Derivatives of Alq<sub>3</sub>

The physical properties of Alq<sub>3</sub> are highly desirable for optoelectronic materials. However, the green emission may not be suitable for all applications. Functionalising the 8-hydroxyquinoline ligand alters the energy level of the HOMO and LUMO. Changing the energy levels of the molecular orbitals also changes the emission wavelength during excitation.<sup>[40]</sup>

Density functional theory calculations have determined that the HOMO resides on the phenoxide ring, while the LUMO is present at the pyridine ring. The LUMO is generally less affected by functionalisation than the HOMO, which is particularly susceptible to change by substitution at the C5 position.<sup>[41]</sup> Electron withdrawing groups attached to the C5 position reduce HOMO density, therefore decreasing the energy level of the HOMO. This increases the separation of the HOMO and LUMO, raising the energy of the transition from the  $\pi$  orbital to the  $\pi^*$  orbital. Raising the transition energy in turn shortens the wavelength of the light emitted compared to unmodified Alq<sub>3</sub>.<sup>[42]</sup> For example, attaching a 2-(4,6-dimethoxy-1,3,5-triazinyl) group at the C5 position (see Fig. 1.17) causes the complex to fluoresce at a wavelength of 490 nm, which is a noticeable colour change from green to blue.<sup>[40]</sup>

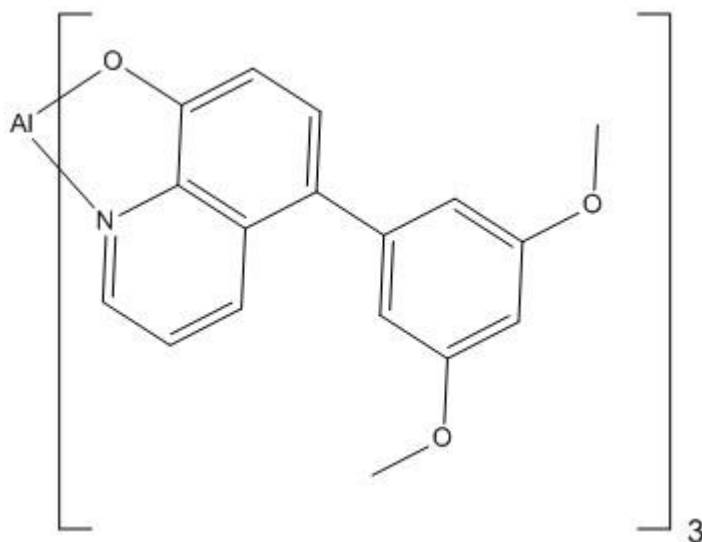


**Figure 1.17:** Diagram of Alq<sub>3</sub> modified with an electron withdrawing group.

Attaching an electron donating group has the opposite effect, as observed when attaching an N,N-dimethylaniline group (see Fig. 1.18). In this case, the HOMO is raised in energy, resulting in a lower energy emission of red light at 616 nm.

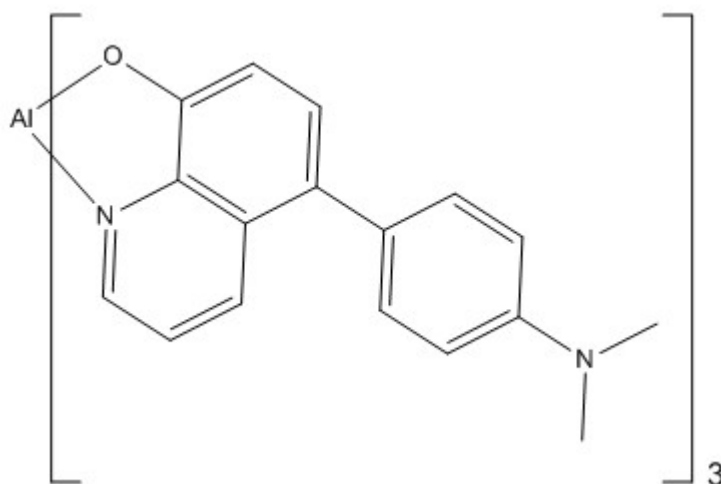


**Figure 1.18:** Diagram of Alq<sub>3</sub> modified with an electron donating group.

Another derivative ligand is 4-morpholinyl-8-hydroxyquinoline (see Fig. 1.19), which displays not only blueshifted emissions (489 nm), but also much more intense fluorescence.<sup>[42]</sup>

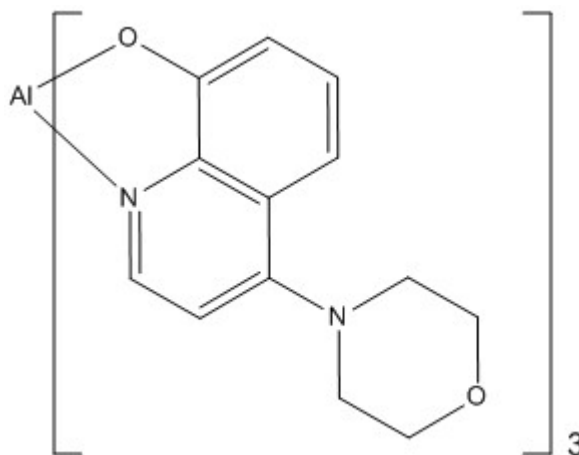


**Figure 1.19:** Tris(4-morpholinyl-8-hydroxyquinolinato)aluminium.

### 1.2.8 Analogues of $Alq_3$

In addition to functionalising the 8-hydroxyquinoline ligand to modify the energy of the molecular orbitals, the aluminium may be substituted for another metal ion. Analogues of  $Alq_3$  vary in the number of coordinated ligands (usually 2-4), depending on the oxidation state of the core atom.

The gallium analogue is  $Gaq_3$ , which contains a Ga(III) ion. The HOMO and LUMO of  $Gaq_3$  are at higher energy levels than those of  $Alq_3$ , but the energy gap is smaller (2.80 eV and 2.86 eV respectively). The lower energy transition results in redshifted fluorescence, so the light emitted from  $Gaq_3$  is much more yellow in colour compared to that of  $Alq_3$ .<sup>[43]</sup>

Another analogue of  $Alq_3$  is  $Znq_2$ . The most obvious difference is that  $Znq_2$  only has two 8-hydroxyquinoline ligands, as it has a Zn(II) core.

Znq<sub>2</sub> has a smaller energy gap between molecular orbitals than Alq<sub>3</sub>, so its fluorescence is redshifted.<sup>[44]</sup> Znq<sub>2</sub> is much more resistant to degradation by air and moisture, drastically improving its shelf-life. The quantum efficiency of Znq<sub>2</sub> is also higher than Alq<sub>3</sub>, meaning the fluorescence of Znq<sub>2</sub> appears much brighter than that of Alq<sub>3</sub> under the same UV excitation source. A sample of Znq<sub>2</sub> is shown in Fig. 1.20.



**Figure 1.20:** Znq<sub>2</sub> under UV excitation.

Mgq<sub>2</sub> emits light at a wavelength of 482 nm, so unlike the previous two analogues presented, Mgq<sub>2</sub> has blueshifted fluorescence relative to Alq<sub>3</sub>.<sup>[45]</sup> Mgq<sub>2</sub> exhibits greater quantum efficiency than Znq<sub>2</sub> in acetonitrile solution (0.45 and 0.03 respectively), but has lower quantum efficiency in the solid state (0.36 and 0.45 respectively).<sup>[46]</sup>

### 1.3 Conclusion

The myriad number of possible conditions a fingerprint may be found in means that no single technique will be appropriate at all times. This is what drives the development of new reagents and methods of

visualising latent fingerprints. The use of dusting powders is a simple way to detect prints and can be drastically improved by addition of fluorescent components. Alq<sub>3</sub> provides a low cost source of intense fluorescence. Due to their importance in the OLED industry, derivatives and analogues of Alq<sub>3</sub> are constantly being developed, giving a choice of emission colour and intensity.

#### **1.4 Scope of this Thesis**

The aim of this project is to develop new dusting powders to visualise latent fingerprints. Magnetite has been selected as the base material due to its ability to adhere to latent prints. Other desirable qualities of magnetite include low cost and low toxicity. In order to improve magnetite as a dusting powder, fluorescent compounds will be added to increase the contrast between the powder and dusting surface. Alq<sub>3</sub> and related compounds have been considered for this purpose. The powders will be tested on different surfaces and applied by different methods, as these are important factors to consider when developing fingerprints.

#### **1.5 References**

1. M. Kralik, L. Nejman "Fingerprints on artifacts and historical items: examples and comments" *J. Ancient Fingerprints* 1, **2007**, 5
2. S. Lundy "FSI: Forensic science investigation (part I)" *CHEM NZ* 98, **2005**, 28-43
3. D. E. Newton, *Forensic Chemistry*, Infobase Publishing **2007**, 12-24

4. D. Crown "The Development of Latent Fingerprints with Ninhydrin"  
J. Criminal Law and Criminology 60, **1969**, 258-264
5. D. W. Herod, E. R. Menzel, "Laser detection of latent fingerprints:  
Ninhydrin followed by zinc chloride," J. Forensic Sci. 27, **1982**, 513
6. V. D'Elia, S. Materazzi, G. Iuliano, L. Niola "Evaluation and  
comparison of 1,2-indanedione and 1,8-diazafluoren-9-one  
solutions for the enhancement of latent fingerprints on porous  
surfaces" Forensic Sci. Int. 254, **2015**, 205-214
7. P. Czekanski, M. Fasola, J. Allison "A Mechanistic Model for the  
Superglue Fuming of Latent Fingerprints" J. Forensic Sci. 51, **2006**,  
1323-1328
8. D. Weaver, E. Clary "A one step fluorescent cyanoacrylate  
fingerprint development technology" National Crime Justice  
Reference Service #144019
9. Y.J. Li, D. Barthès-Biesel, A.-V. Salsac "Polymerization kinetics of  
n-butyl cyanoacrylate glues used for vascular embolization" J.  
Mech. Behav. Biomed. Mater 69, **2017**, 307–317
10. G. Wightman, F. Emery, C. Austin, I. Andersson, L. H Marcus, G. Arju,  
C. Steven "The interaction of fingermark deposits on metal surfaces  
and potential ways for visualisation" School Sci. Eng. Tech.  
University of Abertay, **2015**, 11  
<http://dx.doi.org/10.1016/j.forsciint.2015.01.035> (Accessed on  
14.8.16)

11. O. P. Jasuja, A. Kaur, P. Kumar "Fixing latent fingerprints developed by iodine fuming: a new method" *Forensic Sci. Int.* 223, **2012**, 47-52
12. A. Rawji, A. Beaudoin "Oil Red O Versus Physical Developer on Wet Papers: A Comparative Study" *J. Forensic Ident.* 56, **2006**, 33-56
13. G. S. Sodhi, J. Kaur "Physical developer method for detection of latent fingerprints: A review" *Egypt. J. Forensic Sci.* 6, **2016**, 44-47
14. R. Rohatgi, A. K. Kapoor "Development of latent fingerprints on wet non-porous surfaces with SPR based on basic fuchsin dye" *Egypt. J. Forensic Sci.* 6, **2016**, 179-184
15. N. Jones, M. Stoilovic, C. Lennard, C. Roux "Vacuum metal deposition: developing latent fingerprints on polyethylene substrates after the deposition of excess gold" *Forensic Sci. Int.* 123, **2001**, 5-12
16. D. Newton *Forensic Chemistry, Infobase Publishing*, **2007**, 22-24
17. C. Lennard *Forensic Sciences, Elsevier Ltd*, **2005**, 417
18. L. Bergman, J. McHale, *Handbook of Luminescent Semiconductor Materials, CRC Press*, **2012**, pg1-2 pg145
19. B.I. Stepanov, V.P. Gribkovskii, *Theory of Luminescence, Iliffe Books Ltd* **1968**, 304-315
20. W. Wang, X. Lei, Z. Ye, N. Zhao, H. Yang "The luminescent properties and latent fingerprint identification application of AlN:Ce, Tb phosphors" *J. Alloys Compd.* 705, **2017**, 253-261

21. [https://www.lynnpeavey.com/product\\_info.php?products\\_id=278](https://www.lynnpeavey.com/product_info.php?products_id=278)  
(Accessed 16.11.17)
22. J. Lee, C. Lee, J. Kim "A Magnetically Responsive Polydiacetylene Precursor for Latent Fingerprint Analysis" *ACS Appl. Mater. Interfaces* 8, **2016**, 6245–6251
23. H. Chen, R. Ma, Y. Chen, L. Fan "Fluorescence Development of Latent Fingerprint with Conjugated Polymer Nanoparticles in Aqueous Colloid Solution" *ACS Appl. Mater. Interfaces* 9, **2017**, 4908–4915
24. Y. Li, C. Xu, C. Shu, X. Hou, P. Wu "Simultaneous extraction of level 2 and level 3 characteristics from latent fingerprints imaged with quantum dots for improved fingerprint analysis" *Chinese Chemical Letters* 28, **2017**, 1961-1964
25. C. Xu, R. Zhou, W. He, L. Wu, P. Wu, X. Hou "Fast Imaging of Eccrine Latent Fingerprints with Nontoxic Mn-Doped ZnS QDs" *Anal. Chem.* 86, **2014**, 3279–3283
26. J. A. DeLuca "An Introduction to Luminescence in Inorganic Solids" *J. Chem. Educ.* 8, **1980**, 541-545
27. F. Thorp-Greenwood "An Introduction to Organometallic Complexes in Fluorescence Cell Imaging: Current Applications and Future Prospects" *Organometallics* 31, **2012**, 5686–5692
28. Q. Zhao, C. Huang, F. Li "Phosphorescent heavy-metal complexes for bioimaging" *Chem. Soc. Rev.* 40, **2011**, 2508–2524
29. Y. Wu, J. Wen, H. Li, S. Sun, Y. Xu "Fluorescent probes for recognition of ATP" *Chin. Chem. Lett.* 28, **2017**, 1916–1924

30. T. A. Ruda-Eberenz, A. Nagy, W. James Waldman, and P.K. Dutta  
“Entrapment of Ionic Tris(2,2'-Bipyridyl)Ruthenium(II) in  
Hydrophobic Siliceous Zeolite: O<sub>2</sub> Sensing in Biological  
Environments” *Langmuir*, 24, **2008**, 9140-9147
31. L. Armelao, S. Quicib, F. Barigelletti, G. Accorsic, G. Bottarod,  
M. Cavazzinib, E. Tondelloe “Design of luminescent lanthanide  
complexes: From molecules to highly efficient photo-emitting  
materials” *Coord. Chem. Rev.* 254, **2010**, 487–505
32. T. Liu, B. Campbell, J. Sullivan “Fluorescent Paint for Measurement  
of Heat Transfer in Shock – Turbulent Boundary Layer Interaction”  
*Exp. Therm. Fluid Sci.* 10, **1995**, 101-112
33. T. Tsukamoto, M. Esashi, S. Tanaka “High spatial, temporal and  
temperature resolution thermal imaging method using Eu(TTA)<sub>3</sub>  
temperature sensitive paint” *J. Micromech. Microeng.* 23, **2013**,  
114015
34. B. Wang, J. Hai, Q. Wang, T. Li, Z. Yang “Coupling of Luminescent  
Terbium Complexes to Fe<sub>3</sub>O<sub>4</sub> Nanoparticles for Imaging  
Applications” *Angew. Chem. Int. Ed.* 50, **2011**, 3063 –3066
35. E. Lin, A. Rahmawati, J. Ko, J. Liu “Extraction of yttrium and  
europium from waste cathode-ray tube (CRT) phosphor by  
subcritical water” *Separation and Purification Technology* 192,  
**2018**, 166–175
36. S. A. Bhagat, S. B. Raut, S. J. Dhoble “Study of photophysical  
properties of different metal complexes of Alq<sub>3</sub>” *Luminescence* 28,  
**2013**, 755–759

37. M. Cölle, W. Brütting “Thermal, Structural and photophysical properties of the organic semiconductor Alq<sub>3</sub>” *Phys. Stat. Sol. (a)* 201, **2004**, 1095–1115
38. G. Baldacchini, T. Baldacchini, A. Pace, R. B. Podes “Emission Intensity and Degradation Process of Alq<sub>3</sub> Films” *Electrochem. Solid State Lett.* 8, **2005** 24-26
39. F. Papadimitrakopoulos, X. M. Zhang, D. L. Thomsen, K. A. Higginson “A Chemical Failure Mechanism for Aluminium(III) 8-Hydroxyquinoline Light-Emitting Devices” *Chem. Mater.* 8, **1996**, 1363-1365
40. V. A. Montes, R. Pohl, J. Shinar, P. Anzenbacher Jr. “Effective Manipulation of the Electronic Effects and Its Influence on the Emission of 5-substituted Tris(8-quinolinolate) Aluminium(III) Complexes” *Chem. Eur. J.* 12, **2006**, 4523 – 4535
41. A. Tolkki, K. Kaunisto, J. P. Heiskanen, P. Juha, W. A. E. Omar, K. Huttunen, S. Lehtimäki, O. E. O. Hormi, H. Lemmetyinen “Organometallic tris(8-hydroxyquinoline)aluminium complexes as buffer layers and dopants in inverted organic solar cells” *Thin Solid Films* 520, **2012**, 4475–4481
42. W. A. E. Omar “Synthesis and photophysical properties of aluminium tris-(4-morpholine-8-hydroxyquinoline)” *J. Adv. Res.* 4, **2013**, 525–529
43. F. F. Muhammad, A. I. A. Hapip, K. Sulaiman “Study of optoelectronic energy bands and molecular energy levels of tris(8-hydroxyquinolate) gallium and aluminum organometallic materials

from their spectroscopic and electrochemical analysis" J.

Organometallic Chem. 695, **2010**, 2526-2531

44. T. A. Hopkins, K. Meerholz, S. Shaheen, M. L. Anderson, A. Schmidt, B. Kippelen, A. B. Padias, H. K. Hall Jr., N. Peyghambarian, N. R. Armstrong "Substituted Aluminium and Zinc Quinolates with Blue-Shifted Absorbance/Luminescence Bands: Synthesis and Spectroscopic, Photoluminescence, and Electroluminescence Characterization" Chem. Mater. 8, **1996**, 344-351
45. X. Wang, M. Shao, L. Liu "A facile route to ultra-long bis(8-hydroxyquinoline) magnesium nanoribbons and the fabrication of photoswitch" Thin Solid Films 519, **2010**, 231-234
46. T. Tsuboi, Y. Nakai, Y. Torii "Photoluminescence of bis(8-hydroxyquinoline) zinc( $Znq_2$ ) and magnesium ( $Mgq_2$ )" Cent. Eur. J. Phys. 10, **2012**, 524-528

## Chapter Two: Preparation of Fluorescent Magnetite-based Fingerprinting Powders

### 2.1 Introduction

As described in Chapter One, fingerprinting is a valuable forensic technique. However, some fingerprinting reagents are prohibitively expensive in some parts of the world,<sup>[1]</sup> while other methods, such as cyanoacrylate fuming, have the potential to be hazardous. A fingerprinting reagent based on magnetite would be ideal as it can be acquired from natural sources cheaply and has very low toxicity.

This chapter will detail the preparation and testing of several magnetite-based fluorescent fingerprinting powders. Of the 8-hydroxyquinoline complexes covered in Chapter One,  $\text{Alq}_3$ ,  $\text{Gaqq}_3$ ,  $\text{Znqq}_2$ , and  $\text{Mgqq}_2$  were chosen to be the fluorescent components of the powders, as they are relatively cheap and simple to synthesise.

In order to optimise the formulations, the parameters of each powder were adjusted and tested under various conditions. The ratio of magnetite to fluorescent component was one such parameter, as altering it has a large impact on the physical properties of the powder. The particle size of fingerprinting powders has been shown to affect their ability to visualise fingerprints.<sup>[1]</sup> This is because varying the particle size affects the amount of background staining and amount of particles that are available to adhere to the fingerprint.

Application methods were also compared. One of the advantages of magnetite is that it is magnetic. This allows it to be applied by either conventional zephyr brush or magnetic applicator. Due to their nature, magnetic brushes are somewhat more user-friendly, as they can easily be cleaned, reducing the risk of contaminating the fingerprinting powder.

Fluorescent compounds may lose their fluorescent properties when exposed to light through a process known as photobleaching. This occurs because the absorption of photons can catalyse the degradation of these compounds.<sup>[2]</sup> Moisture has also been shown to play a role in the loss of fluorescence in 8-hydroxyquinoline compounds,<sup>[3][4]</sup> so the atmospheric stability of each of the complexes was investigated.

Due to the wide variety of possible conditions fingerprints can be found under, it is important to use the right visualisation method for the situation. In order to ascertain the surface upon which the fingerprinting powders perform best, the powders were tested on a range of materials. Drink cans and glass microscope slides were used to simulate common surfaces, while plastic overhead-projector sheets and pieces of thermal receipt paper were used to test the efficacy of the powders on surfaces that are designed to avoid dust particulate build-up.

## 2.2 Experimental

### 2.2.1 Materials

**Table 2.1:** Reagents and Solvents

| <b>Name</b>  | <b>Source</b>   |
|--|---|
| Sulfuric acid  | Ajax Finechem (analytical grade 98%)                            |
| 8-Hydroxyquinoline                                   | Honeywell Riedel-de Haën AG                                     |
| Hydrochloric acid                                    | Merck (Emsure grade 36%)  |
| Ammonia  | Merck (Emsure grade 30%)  |
| Dichloromethane                                      | Merck (Emsure grade)  |
| Ethanol (absolute)                                   | University of Waikato Science Store (drum grade)                |
| $\text{Al}(\text{NO}_3)_3 \cdot 9\text{H}_2\text{O}$ | BDH Chemicals Ltd   |
| Gallium  | GalliumSource (99.99% pure)                                     |
| $\text{Zn}(\text{SO}_4)_2 \cdot 7\text{H}_2\text{O}$ | Scharlau Chemie   |
| $\text{MgCl}_2$ (anhydrous)                          | Merck (>98% pure)   |
| Magnetite  | Inoxia (>98.1% pure, sourced from naturally occurring deposits) |

**Table 2.2:** Equipment

| <b>Name</b>                             | <b>Source</b> |
|---|---------------|
| “The Breeze” Zephyr Brush               | CleanSearch   |
| Standard Magnetic Applicator            | Sirchie       |
| 125 $\mu\text{m}$ Laboratory Test Sieve | Endecotts Ltd |
| 65 $\mu\text{m}$ Laboratory Test Sieve  | Endecotts Ltd |
| Ultraviolet Lamp, 365 nm Tube           | Uvitec        |
| “BX51” Petrographic Microscope          | Olympus       |

**Table 2.3:** Test Surfaces

| <b>Type</b>               | <b>Product</b>                       |
|---------------------------|--------------------------------------|
| Soda Can                  | V Sugar Free                         |
| Microscope Slide          | Fronine Microscope Slides 26 x 76 mm |
| Over-Head-Projector Sheet | OfficeMax OHP Transparency Film A4   |
| Thermal Receipt Paper     | TMA Eftpos Roll 57 x 50 mm           |

### 2.2.2 Synthesis of $Alq_3$

$Alq_3$  was synthesised using a modified literature method.<sup>[5]</sup> Sulfuric acid (12.5 mL, 98%) was added to distilled water (237.5 mL). 8-Hydroxyquinoline (25 g) was added and stirred at room temperature until dissolved. In a separate beaker,  $Al(NO_3)_3 \cdot 9H_2O$  (21.5 g) was added to distilled water (150 mL) and stirred until dissolved. The solution of aluminium nitrate was added to the 8-hydroxyquinoline solution and stirred (10 min). Ammonia (50 mL, 30%) was added dropwise while stirring. The yellow precipitate was filtered and then washed with distilled water (100 mL) while on the filter. The remaining solid was dried overnight at 50°C. The final mass of the solid was 27 g, which corresponds to a yield of 102% (discussed in section 2.3.1).

### 2.2.3 Synthesis of $Gaq_3$

$Gaq_3$  was prepared using a modified literature method.<sup>[6]</sup> Hydrochloric acid (30 mL, 36%) and distilled water (200 mL) were added to a round bottom flask in a reflux setup. Gallium metal (0.69 g) was added and the vessel was heated gently on a hotplate (48 hours, 60°C). The solution was transferred to a beaker once the gallium was dissolved. 8-Hydroxyquinoline (5 g) was added and stirred until dissolved while cooling. Ammonia (60 mL, 30%) was added dropwise. The precipitate was filtered, then washed with distilled water (100 mL) while on the filter. The remaining yellow solid was dried in an oven overnight at 50°C. The final

mass of the solid was 5.9 g, which corresponds to a yield of 119% (discussed in section 2.3.1).

#### 2.2.4 Synthesis of $Znq_2$

$Znq_2$  was prepared using a modified literature method.<sup>[7]</sup>  $ZnSO_4 \cdot 7H_2O$  (2.88 g) and 8-hydroxyquinoline (3.33 g) were added to distilled water (150 mL). Sulfuric acid (10 mL, 98%) was added and the mixture was stirred (10 min) before addition of ammonia (50 mL, 30%). The resulting precipitate was filtered and washed with distilled water (100 mL) while on the filter. The remaining yellow solid was dried in an oven overnight at 50°C. The final mass of the solid was 3.2 g, which corresponds to a yield of 90%.

#### 2.2.5 Synthesis of $Mgq_2$

$Mgq_2$  was prepared using a modified literature method.<sup>[7]</sup>  $MgCl_2$  (3.3 g) and 8-hydroxyquinoline (5 g) were added to a beaker containing distilled water (150 mL). The dark brown solution was stirred (10 min), before addition of ammonia (50 mL, 30%). The yellow precipitate was filtered and washed with distilled water (100 mL) while on the filter. The yellow solid was dried overnight at 50°C. The final mass of the solid was 2 g, which corresponds to a yield of 18%.

### 2.2.6 Preparation of Fluorescent Fingerprint Powders

Fluorescent activity was imparted to magnetite powder by coating the surface of the particles with a fluorescent compound. This was achieved through the following method: To a round bottom flask (500 mL), magnetite, the fluorescent compound (10 g of material total, see Table 2.4 for the mass ratio of magnetite to fluorescent compound), and dichloromethane (150 mL) were added. The fluorescent compound dissolved in the dichloromethane, while the magnetite remained undissolved. The magnetite was coated by the fluorescent compound during rotary evaporation.

In order to test the impact of particle size, some powders were separated into different size fractions using 125  $\mu\text{m}$  and 65  $\mu\text{m}$  sieves. The powders were placed in separate jars according to their sizes.

Table 2.4 displays the composition of the fingerprint powders as mass percentages. Each formulation was given a label made of three parts. The percentage indicates the amount of fluorescent component by mass percentage. The second part denotes the compounds present. AM, GM, ZM, and MgM, refers to  $\text{Alq}_3$ ,  $\text{Gaq}_3$ ,  $\text{Znq}_2$ , and  $\text{Mgq}_2$ , magnetite powders respectively. Some of the powders were separated into size fractions; for those powders, the third part of the label refers to the size of the particles. Powders that contain “<65  $\mu\text{m}$ ” in their label have a maximum particle size of 65  $\mu\text{m}$ , while powders with “>125  $\mu\text{m}$ ” in their label have a minimum particle size of 125  $\mu\text{m}$ . Powders with “65-125  $\mu\text{m}$ ” in their label have a minimum particle size of 65  $\mu\text{m}$  and a maximum particle size of 125  $\mu\text{m}$ .

**Table 2.4:** List of Powder Formulations

| <b>List of Powder Formulations</b> |                             |
|------------------------------------|-----------------------------|
| 80% AM                             | 10% AM >125 $\mu\text{m}$   |
| 60% AM                             | 20% GM                      |
| 40% AM                             | 10% GM                      |
| 20% AM                             | 20% MgM                     |
| 10% AM                             | 20% ZM                      |
| 5% AM                              | 10% ZM                      |
| 20% AM <65 $\mu\text{m}$           | 20% ZM <65 $\mu\text{m}$    |
| 20% AM 65-125 $\mu\text{m}$        | 20% ZM 65-125 $\mu\text{m}$ |
| 20% AM >125 $\mu\text{m}$          | 20% ZM >125 $\mu\text{m}$   |
| 10% AM <65 $\mu\text{m}$           | 10% ZM <65 $\mu\text{m}$    |
| 10% AM 65-125 $\mu\text{m}$        | 10% ZM 65-125 $\mu\text{m}$ |

### 2.2.7 Application Method

The left thumb of the author was used to apply fingerprints to the test surfaces. The thumb was coated in sebum by touching it to the forehead before fingerprint application. This method is similar to that of a previous study.<sup>[1]</sup>

When using the zephyr brush as the applicator, the powder was deposited by gently brushing over the latent fingerprints. A separate brush was used to avoid cross contamination between powders. For the magnetic brush, the powder was picked up and then the brush was tapped against the side of the sample jar to shake off loose powder before applying powder to the print. The brush was emptied into the storage container by raising the plunger. The empty brush was then used to pick up excess powder from the dusted print.

### 2.2.8 Atmospheric Reactivity Tests

To gauge the stability of the fluorescent compounds under standard conditions, a sample (0.1 g) of each compound was left on a watch glass in a fume hood with the light on. After one month, each sample was checked for fluorescence by irradiating the samples with UV light. The fluorescence of the samples was compared to that of samples that were kept in sealed jars and placed in a dark cupboard as a control.

### 2.2.9 Assessment of Powders

Photographs were taken of the fingerprints after dusting powder was applied under visible light and then in the dark underneath a UV lamp (365 nm). To assess the efficacy of each powder for a set of conditions, quality grades were devised. The quality grade takes into account the brightness of the fluorescence, contrast against the background surface, and clarity of fingerprint details. Table 2.5 displays the possible quality grades and a description of what is required to achieve each grade.

**Table 2.5:** Quality Grades

| <b>Quality Grade</b> | <b>Requirement</b>          |
|----------------------|-----------------------------|
| 0                    | Fingerprint not visible     |
| 1                    | Fingerprint outline visible |
| 2                    | Some details present        |
| 3                    | Fingerprint mostly clear    |
| 4                    | All details visible         |
| 5                    | Near Perfect                |

## 2.3 Results

### 2.3.1 Syntheses

The fluorescent powders,  $\text{Alq}_3$ ,  $\text{Gaq}_3$ ,  $\text{Znq}_2$ , and  $\text{Mgq}_2$ , were all bright yellow-green in appearance. The yields of  $\text{Alq}_3$  and  $\text{Gaq}_3$  were greater than 100%. The reagents used were of good quality, so impurities in the final products are unlikely to be the cause of the excess mass.

Water-weight was also an improbable cause, as the samples were dried thoroughly. 8-Hydroxyquinoline has the ability to hydrogen bond due to the presence of oxygen atoms. Water of crystallisation may be responsible for the yield being above 100%, as this hydrogen bonding potential may cause water molecules to be incorporated into the crystal lattice. Hydrated  $\text{Alq}_3$  has been reported,<sup>[8]</sup> but there has been little investigation into hydrated  $\text{Gaq}_3$  species.

Compared to the other syntheses, the  $\text{Mgq}_2$  preparation gave a very low yield of approximately 18%.  $\text{Mgq}_2$  has more ionic character than the other compounds, as the  $\text{Mg}^{2+}$  ion has a lower electronegativity than the  $\text{Al}^{3+}$ ,  $\text{Ga}^{3+}$ , or  $\text{Zn}^{2+}$  ions, which results in greater solubility in aqueous media. Using less solvent and a lower temperature would decrease the solubility of the  $\text{Mg}^{2+}$ , potentially improving the yield. An alternative solvent could also be used to improve the yield.

### 2.3.2 Fingerprint Tests

Table 2.6 details the conditions of each test performed, as well as the quality grades. 'Brush' refers to whether the powders were applied via

a zephyr brush or a magnetic brush. 'Surface' refers to the surface the fingerprint was laid upon. The abbreviations 'C', 'OHP', 'MS', and 'RP' refer to soft drink cans, plastic overhead projector sheets, microscope slides, and thermal receipt paper, respectively. The columns 'UV' and 'Visible' contain the quality grades assigned to each powder under UV light and visible light, respectively.

**Table 2.6:** Conditions of Fingerprinting Tests

| <b>Label</b> | <b>Formulation Used</b> | <b>Brush</b> | <b>Surface</b> | <b>UV</b> | <b>Visible</b> |
|--------------|-------------------------|--------------|----------------|-----------|----------------|
| 1            | 20% AM                  | Zephyr       | C              | 4         | 2              |
| 2            | 10% AM                  | Zephyr       | C              | 4         | 2              |
| 3            | 20% ZM                  | Zephyr       | C              | 3         | 3              |
| 4            | 10% ZM                  | Zephyr       | C              | 3         | 4              |
| 5            | 20% AM                  | Zephyr       | OHP            | 2         | 2              |
| 6            | 10% AM                  | Zephyr       | OHP            | 1         | 2              |
| 7            | 20% ZM                  | Zephyr       | OHP            | 2         | 2              |
| 8            | 10% ZM                  | Zephyr       | OHP            | 1         | 2              |
| 9            | 20% AM                  | Zephyr       | MS             | 3         | 2              |
| 10           | 10% AM                  | Zephyr       | MS             | 2         | 2              |
| 11           | 20% ZM                  | Zephyr       | MS             | 2         | 2              |
| 12           | 10% ZM                  | Zephyr       | MS             | 2         | 2              |
| 13           | 20% MgM                 | Zephyr       | C              | 2         | 3              |
| 14           | 20% MgM                 | Zephyr       | OHP            | 1         | 2              |
| 15           | 20% MgM                 | Zephyr       | MS             | 2         | 2              |
| 16           | 20% AM                  | Zephyr       | RP             | 2         | 2              |
| 17           | 10% AM                  | Zephyr       | RP             | 2         | 2              |
| 18           | 20% ZM                  | Zephyr       | RP             | 1         | 2              |
| 19           | 10% ZM                  | Zephyr       | RP             | 1         | 2              |
| 20           | 20% AM <65 $\mu$ m      | Zephyr       | C              | 3         | 3              |
| 21           | 20% AM 65-125 $\mu$ m   | Zephyr       | C              | 4         | 2              |
| 22           | 20% AM >125 $\mu$ m     | Zephyr       | C              | 5         | 2              |
| 23           | 10% AM <65 $\mu$ m      | Zephyr       | C              | 4         | 1              |
| 24           | 10% AM 65-125 $\mu$ m   | Zephyr       | C              | 4         | 1              |
| 25           | 10% AM >125 $\mu$ m     | Zephyr       | C              | 4         | 1              |
| 26           | 20% GM                  | Zephyr       | C              | 2         | 3              |
| 27           | 10% GM                  | Zephyr       | C              | 3         | 4              |
| 28           | 20% GM                  | Magnetic     | C              | 2         | 4              |
| 29           | 10% GM                  | Magnetic     | C              | 2         | 3              |
| 30           | 20% GM                  | Magnetic     | MS             | 2         | 2              |
| 31           | 20% AM                  | Magnetic     | MS             | 2         | 2              |

|           |                             |        |   |   |     |
|-----------|-----------------------------|--------|---|---|-----|
| <b>32</b> | 20% ZM <65 $\mu\text{m}$    | Zephyr | C | 1 | 1   |
| <b>33</b> | 20% ZM 65-125 $\mu\text{m}$ | Zephyr | C | 2 | 2   |
| <b>34</b> | 20% ZM >125 $\mu\text{m}$   | Zephyr | C | 3 | 2   |
| <b>35</b> | 10% ZM <65 $\mu\text{m}$    | Zephyr | C | 1 | 2   |
| <b>36</b> | 10% ZM 65-125 $\mu\text{m}$ | Zephyr | C | 2 | 2   |
| <b>37</b> | 10% ZM >125 $\mu\text{m}$   | Zephyr | C | 2 | 0.5 |

### 2.3.3 Effects of Fluorescent Component

Of the fluorescent compounds tested, the GM powders showed the least intense fluorescence. The ZM powders were the brightest, though only by a small margin. All of the powders displayed adequate fluorescence for visualising prints, so the intensity of fluorescence was of minor importance.

The MgM powder had bright fluorescence, but excessive background staining (possibly due to low affinity for the fingerprint) made it difficult to resolve the features of the fingerprint (see Fig. 2.1).

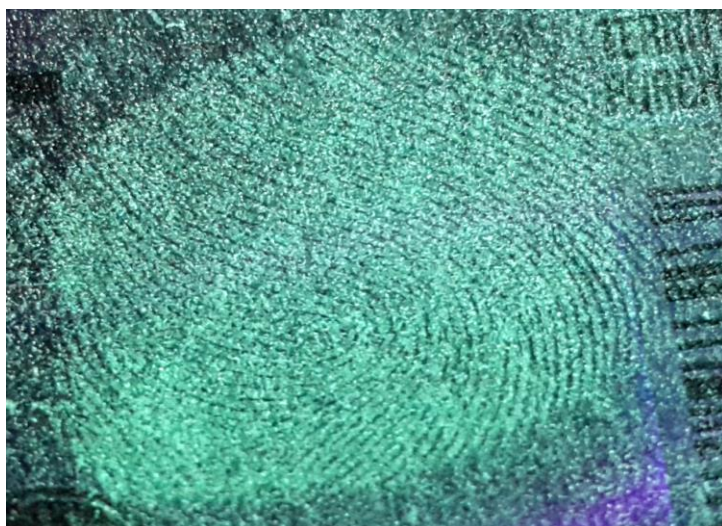


**Figure 2.1:** Fingerprint under UV light visualised by 20% MgM applied via zephyr brush. Note the large amount of background staining.

Although the GM powders had the lowest intensity of fluorescence, they were still clearly visible under UV light. GM powders gave less background staining than MgM powders, but some features were still obscured (see Fig. 2.2).

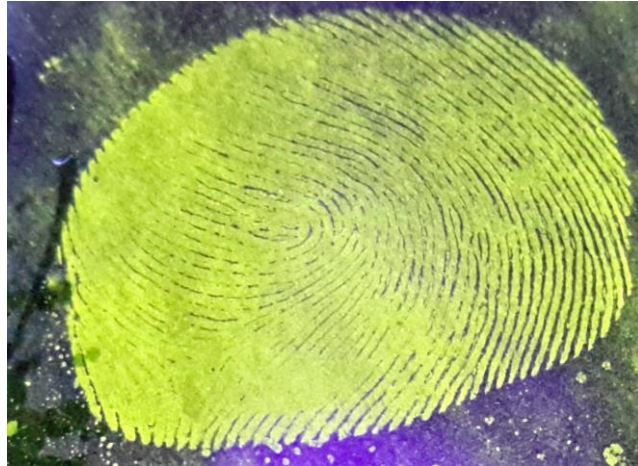


**Figure 2.2:** Fingerprint under UV light visualised by 20% GM applied via zephyr brush.

The AM and ZM powders had similar performance with good fluorescence intensity and generally low background staining (refer to Table 2.6). The ZM powders had slightly more intense fluorescence, but the AM powders gave superior quality grades. For example, the 10% and 20% AM powders applied to cans via zephyr brush both gave quality grades of 4, but under the same conditions, the 10% and 20% ZM powders only gave quality grades of 3.

In most cases, the fingerprints were easier to resolve under UV excitation due to greatly improved contrast between the dusting surface and fingerprint (see Fig. 2.3).



**Figure 2.3:** Fingerprints under visible light (top) and UV light (bottom) visualised by 20% AM applied via zephyr brush.

The GM powders unexpectedly gave better contrast under visible light than under UV excitation in some cases (see Fig. 2.4) due to powder settling in the furrows (the area between the ridges) of the fingerprint.



**Figure 2.4:** Fingerprints under UV light (left) and visible light (right) visualised by 10% GM applied via magnetic brush.

Fingerprints were laid on two microscope slides and visualised using a magnetic brush to apply the 10% GM powder on one slide and the 20% GM powder on the other. Examination of the fingerprints using a petrographic microscope revealed that loose  $\text{Gaq}_3$  was present in both powders (see Fig. 2.5). The GM powder was found mainly in the ridges of the fingerprint, but the  $\text{Gaq}_3$  was found in both the ridges and farrows. This suggested that the  $\text{Gaq}_3$  had little affinity for the features of the fingerprint and that the magnetite is an essential component in the dusting powder, as it imparts selectivity for the fingerprint ridges.

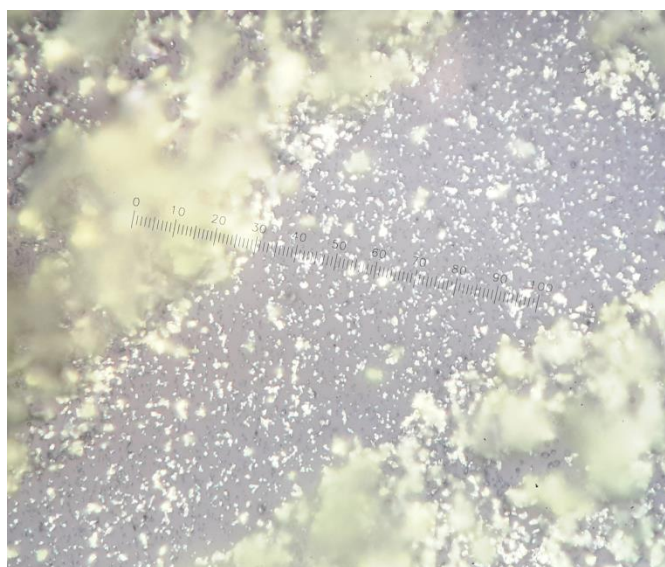


**Figure 2.5:** 500x magnification of a fingerprint visualised by 20% GM applied via magnetic brush. The farrow of the fingerprint is in focus, while the ridges are out of focus due to the narrow depth of field.

#### 2.3.4 Atmospheric Reactivity

$\text{Alq}_3$  is known to degrade under standard conditions to a dark compound that does not fluoresce.<sup>[3]</sup> The samples of  $\text{Alq}_3$  and  $\text{Gaq}_3$

changed from bright yellow to a darker yellow-orange colour after being exposed to light and air for an extended period. The degraded compounds did not fluoresce at all. Previous studies<sup>[9]</sup> have shown that the energy level of Alq<sub>3</sub>'s HOMO is higher than that of Gaq<sub>3</sub>, making Alq<sub>3</sub> more resistant to oxidation. However, this difference was inconsequential for the purpose of this thesis.

The Znq<sub>2</sub> and Mgq<sub>2</sub> compounds did not degrade and showed little indication of diminished fluorescence. It has been suggested that the more closely packed crystal structure of Znq<sub>2</sub> drastically improves its resistance to oxidation compared to tris(8-hydroxyquinolato) complexes. In an experiment by Duvenhage *et al.*,<sup>[10]</sup> samples of Alq<sub>3</sub> and Znq<sub>2</sub> were exposed to UV light for 400 hours. The fluorescent activity of the samples was measured and it was found that the fluorescence intensity of the samples decreased by 80% and 30% for Alq<sub>3</sub> and Znq<sub>2</sub>, respectively.

Mgq<sub>2</sub> is also known for its stability. In a study by Shen *et al.*,<sup>[11]</sup> aluminium alloys high in magnesium were coated in an epoxy containing magnesium and 8-hydroxyquinoline. Conventional anti-corrosion coatings contain magnesium particles, which act as sacrificial anodes to protect the alloy underneath. However, these particles often react to form Mg(OH)<sub>2</sub>, which may react further to form water-soluble salts such as MgCl<sub>2</sub>. In the case of the coating containing 8-hydroxyquinoline, Mgq<sub>2</sub> formed instead, which is much more resistant to further reaction.

### 2.3.5 Effects of Test Surface

The powders were tested on four different surfaces. The aluminium soda cans used were silver with minimal printed graphics. This meant that the colourful graphics would not obscure the details of the visualised fingerprints. The cans were selected as a test surface because cans are very common objects. The microscope slides chosen were conventional glass slides for an optical microscope. The slides were used to represent more common glass surfaces such as windows or tempered glass furniture. The OHP sheets were used to test the limits of the powders, as the sheets were coated in anti-static agents by the manufacturer to reduce dust build-up (as it would impair the visibility of slides printed on the sheets). The thermal receipt paper used was another surface designed to avoid gathering dust, as stray particulates can reduce the lifetime of receipt printers. The receipt paper was also picked because receipts can be of significant forensic importance.<sup>[12][13][14]</sup>

The dusting surface had a noticeable impact on quality, with drink cans giving the best results. The microscope slides offered the next best level of quality, while the plastic OHP sheets (see Fig. 2.6) and thermal receipt paper gave poor results. It is hypothesised that porosity and hydrophilicity are the main properties of the surface that affect the potential quality of the fingerprint.

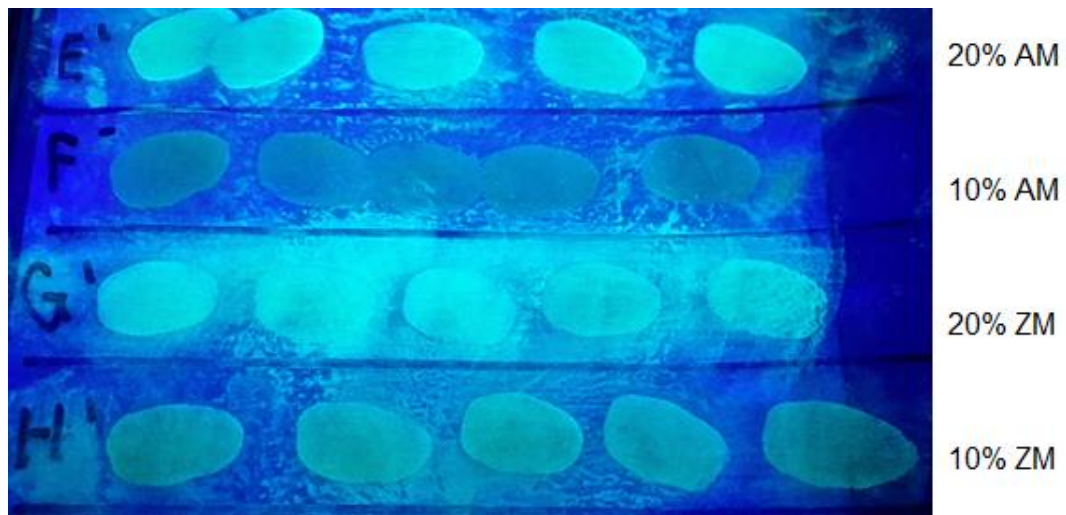


**Figure 2.6:** Fingerprints on a plastic OHP sheet under UV light visualised by 20% AM, 10% AM, 20% ZM, and 10% ZM applied via zephyr brush.

### 2.3.6 Effects of Ratio

In preliminary tests the 80% AM, 60% AM, 40% AM, and 5% AM powders gave vastly inferior results to the 20% AM and 10% AM powders, so they were excluded from the main battery of tests. The excluded powders generally gave poor contrast due to either weak fluorescence or limited adhesion to the fingerprint. The 20% AM and 10% AM powders had very similar performance, but the 20% AM powder generally gave better results in the cases where their quality grades differed. The 10% GM powder outperformed the 20% GM powder when applied to drink cans with a zephyr brush. Further testing could be performed to confirm which ratio is superior, however Gaq<sub>3</sub> powders are much more expensive than Alq<sub>3</sub> powders (due to the cost of gallium compared to aluminium<sup>1</sup>) while

<sup>1</sup> Metal prices vary based on the economic climate and source, but aluminium is usually a few dollars per kilogram, while gallium may be several hundred dollars per kilogram.

having lower efficacy, so the venture is unnecessary. Only one formulation using  $Mgq_2$  was tested as the 20% MgM powder performed poorly on all test surfaces. Although their performance was similar, the 20% ZM powder had slightly improved performance over the 10% ZM powder. Additional testing would be needed to confirm this.

### 2.3.7 Effects of Application Method

The zephyr brush gave all round better results than the magnetic brush. Fingerprints dusted with the magnetic brush were often damaged and had reduced contrast due to excessive background staining (see Fig. 2.7).



**Figure 2.7:** Fingerprints under UV light visualised by 10% GM applied via magnetic brush. Background staining made the prints very difficult to resolve.

In the case of test **28** (20% GM powder applied to a can via magnetic brush), the background staining was so intense, that reasonable contrast was achieved because the area around the print was fluorescing brighter than the magnetite laden print (see Fig. 2.8).



**Figure 2.8:** Fingerprint under UV light visualised by 20% GM applied via magnetic brush. Note the damage towards the left of the fingerprint caused by the magnetic brush.

### 2.3.8 Effects of Particle Size

In the particle size experiments for the AM powders (experiments **20-25**), the powders with larger particle sizes gave the best results, with the 20% AM 65-125  $\mu\text{m}$  and 20% AM >125  $\mu\text{m}$  powders achieving quality grades of 4 and 5, respectively. This is possibly due to reduced background staining, as smaller particles will readily adhere to the dusting surface as well as the fingerprint, while larger particles are brushed away (see Fig. 2.9). This suggests the  $\text{Alq}_3$ /magnetite fingerprinting reagent has a greater affinity for fingerprints than the dusting surface.

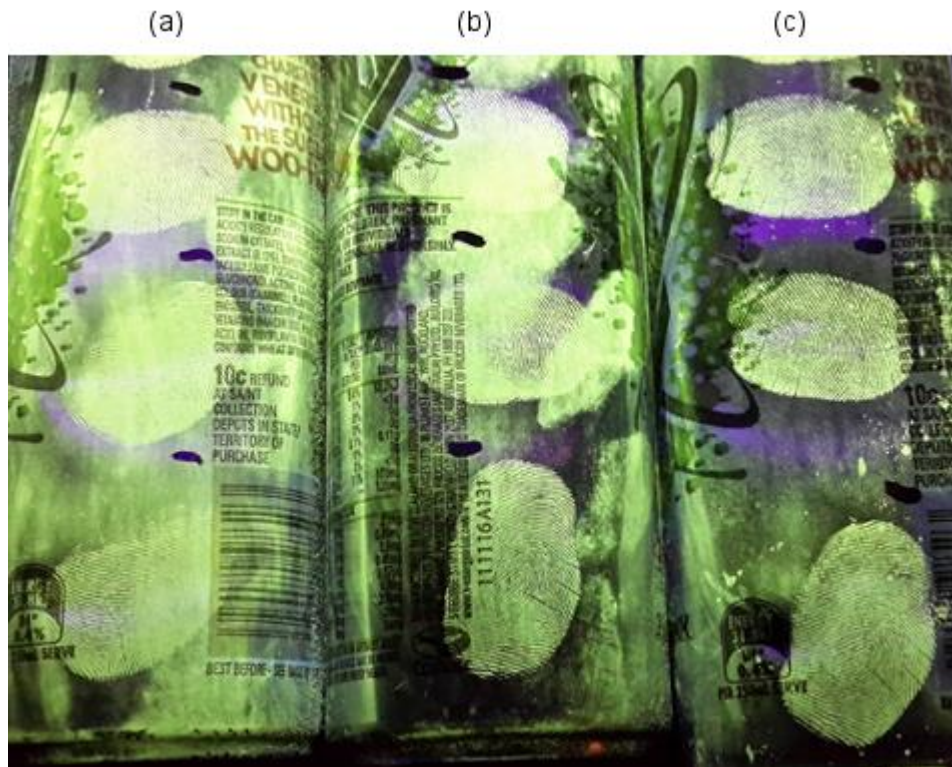


**Figure 2.9:** Fingerprints on cans under UV light visualised by 20% AM <math><65\ \mu\text{m}</math> (a), 20% AM <math>65\text{-}125\ \mu\text{m}</math> (b), and 20% AM <math>>125\ \mu\text{m}</math> (c) powders applied via zephyr brush.

The 20% AM <math><65\ \mu\text{m}</math> powder gave a quality grade of 3 under UV light, which is lower than that of all other 20% AM powder variations (including the 20% AM powder that was not sorted into size fractions). This was likely due to the higher abundance of very small particles that caused background staining. The 20% AM <math>>125\ \mu\text{m}</math> powder gave the best results under UV excitation out of the entire study (see Fig. 2.10).



**Figure 2.10:** Close up of a fingerprint under UV light visualised by 20% AM >125  $\mu\text{m}$  applied via zephyr brush. The black circle on the image highlights some of the level three structures visible (level three fingerprint structures are described in section 1.2.4).

Some level three structures of fingerprints were visible in fingerprints visualised by the 20% AM >125  $\mu\text{m}$  powder, which may allow for the generation of pore maps, increasing the quantity of information each fingerprint can give. The 10% AM powders sorted into size fractions did not show the same variations in performance as the 20% AM powders, as they all gave quality grades of 4 under UV light.

The particle size experiments for the ZM powders (experiments **32-37**) exhibited the same trend as the AM powders, as the powders with the larger particle sizes gave the best results under UV light. The 20% ZM <65  $\mu\text{m}$  and 10% ZM <65  $\mu\text{m}$  powders suffered from heavy background staining far more than the AM equivalents, suggesting that the AM

powders had a greater affinity for fingerprints than the ZM powders. The 10% ZM >125  $\mu\text{m}$  powder had reduced background staining compared to the powders with smaller particle sizes, but was nearly invisible under visible light. Fig. 2.11 shows a comparison of the 10% ZM powders sorted by particle size.

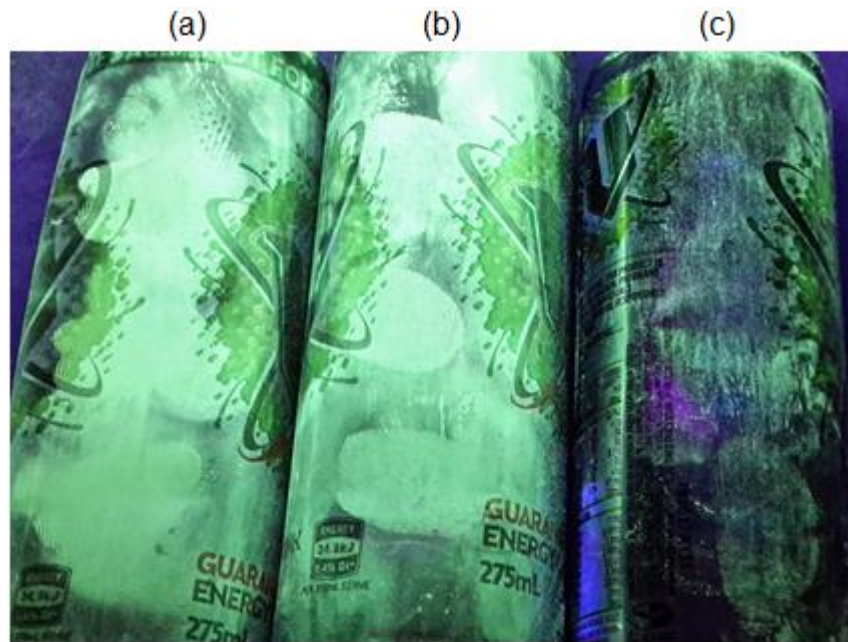


**Figure 2.11:** Fingerprints under UV light visualised by 10% ZM <65  $\mu\text{m}$  (a), 10% ZM 65-125  $\mu\text{m}$  (b), and 10% ZM >125  $\mu\text{m}$  (c) applied via zephyr brush.

## 2.4 Discussion

Under the same conditions, the AM powders proved to have superior performance compared to equivalent powders with different fluorescent components, with the 20% AM >125  $\mu\text{m}$  variant being the best of all. The GM and MgM powders caused significant background staining that obscured the features of the fingerprints. Fingerprints visualised by

the ZM powders were of similar quality to those visualised by the AM powders, but often had more flaws per fingerprint.

The AM powders gave the best results in this study, but the ZM powders did not lose their fluorescence under standard conditions, while performing almost as well as the AM powders. This stability would improve the shelf-life of the fingerprint powder, which may result in reduced cost in the long term, as the powder would not need to be replaced as it aged.

All of the surfaces tested were fairly non-porous, but gave varying results. The cans gave good results, while the other surfaces rarely allowed for high quality visualisation. Fingerprints visualised on the thermal paper and OHP sheets were of especially low quality, but this was to be expected as these materials are designed to avoid accumulating dust particulates. More testing, on a wider variety of surfaces, would have to be done to confirm the ideal surface to use the powders on.

The ratio of fluorescent compound to magnetite was very important, as it had a marked effect on the physical properties of the fingerprint powder. The ideal ratio was not confirmed, but was found to be roughly between 10% and 20% fluorescent compound to magnetite by mass. Excess fluorescent compound decreased the ability of the powder to adhere to fingerprints, while too little resulted in weak fluorescence.

The zephyr brush was found to be the best means of application, as the magnetic brush caused background staining that made it difficult to identify the fingerprints. Changing the powder or dusting surface had little impact on the background staining effect of the magnetic brush. Magnetic

brushes are purported to be less destructive than traditional brushes,<sup>[15]</sup> in contrast to the findings of this study. It is likely that nanoparticle fingerprinting powders are necessary to achieve ideal results with a magnetic brush, while the powders tested in this thesis had particle sizes in the micron range. It could also be possible that the selectivity of the powders for fingerprints was too poor to use with a magnetic brush.

Separating the powders into different size ranges had a profound effect on the performance of the powders. In a study by Gürbüz *et al.*,<sup>[16]</sup> the effects of surface porosity and magnetite particle size on the clarity of visualised fingerprints were investigated. It was found that the powders with smaller particle sizes caused heavy background staining, reducing contrast, while the powder with the largest particle size lacked the ability to stain the fingerprint effectively. The conclusion drawn from these findings was that the presence of some small particles was needed to stain the fingerprint, but too many caused overstaining.

In this study, similar issues with smaller particle sizes and background staining were encountered. However, in contrast to the results of this thesis, the Gürbüz *et al.* study found that magnetite powders with average particle sizes ranging from 57-67  $\mu\text{m}$  gave the best results. In this thesis, the powders with minimum particle sizes greater than 125  $\mu\text{m}$  gave the best contrast. It should be noted that powders studied in the Gürbüz *et al.* study were made of magnetite, without any fluorescent component, and were applied via magnetic brush only.

## 2.5 Conclusion

Various fluorescent 8-hydroxyquinoline compounds were deposited on magnetite powder and tested for their ability to visualise latent fingerprints. The powders containing Alq<sub>3</sub> and Znq<sub>2</sub> showed the most promise. Further development of these powders could allow for the creation of cheap and easy-to-synthesise fingerprint visualisation reagents.

## 2.6 References

1. T. Thonglon, N. Chaikum "Magnetic Fingerprint Powder from a Mineral Indigenous to Thailand" *J. Forensic Sci.* **55**, **2010**, 1343-1346
2. <https://www.microscopyu.com/references/fluorophore-photobleaching> (Accessed on 10.1.18)
3. G. Baldacchini, T. Baldacchini, A. Pace, R. B. Podes "Emission Intensity and Degradation Process of Alq<sub>3</sub> Films" *Electrochem. Solid State Lett.* **8**, **2005** 24-26
4. F. Papadimitrakopoulos, X. M. Zhang, D. L. Thomsen, K. A. Higginson "A Chemical Failure Mechanism for Aluminium(III) 8-Hydroxyquinoline Light-Emitting Devices" *Chem. Mater.* **8**, **1996**, 1363-1365
5. S. A. Bhagat, S. B. Rautb, S. J. Dhoble "Study of photophysical properties of different metal complexes of Alq<sub>3</sub>" *Luminescence* **28**, **2013**, 755–759

6. L. Wang, X. Jiang, Z. Zhang, S. Xu “Organic thin film electroluminescent devices using Gaq3 as emitting layers” *Displays* 21, **2000**, 47–49
7. T. Tsuboi, Y. Nakai, Y. Torii “Photoluminescence of bis(8-hydroxyquinoline) zinc ( $Znq_2$ ) and magnesium ( $Mgq_2$ )” *Cent. Eur. J. Phys.* 10, **2012**, 524-528
8. M. S. Xu, J. B. Xu “Nanoscale study on origins of the bright clusters in/on moisture-exposed tris(8-hydroxyquinoline) aluminium thin films” *Synthetic Metals* 145, **2004**, 177-182
9. F. F. Muhammad, A. I. A. Hapip, K. Sulaiman “Study of optoelectronic energy bands and molecular energy levels of tris(8-hydroxyquinolate) gallium and aluminum organometallic materials from their spectroscopic and electrochemical analysis” *Journal of Organometallic Chemistry* 695, **2010**, 2526-2531
10. M. M. Duvenhage, J. J. Terblans, M. Ntwaeborwa, H. C. Swart “XPS investigation of the photo degradation of  $Znq_2$  green organic phosphor” *Physica B* 480, **2016**, 141–146
11. S. Shen, Y. Zuo, X. Zhao “The effects of 8-hydroxyquinoline on corrosion performance of a Mg-rich coating on AZ91D magnesium alloy” *Corrosion Sci.* 76, **2013**, 275-283
12. W. Wise *Indonesia’s War on Terror*, United States – Indonesia Society, **2005**, 9
13. <http://lifestyle.inquirer.net/84183/a-lesson-gone-wrong/> (Accessed on 11.1.18)

14. <https://phys.org/news/2014-10-technology-hidden-properties-receipts-fingerprint.html> (Accessed on 11.1.18)
15. C. Lennard *Forensic Sciences*, Elsevier Ltd , **2005**, 417
16. S. Gürbüz, B. Özmen Monkul, T. Ipeksaç, M. Gürtekin Seden, M. Erol “A Systematic Study to Understand the Effects of Particle Size Distribution of Magnetic Fingerprint Powders on Surfaces with Various Porosities” *J. Forensic Sci.* 60, **2015**, 727-736

## Chapter Three: Attempted Synthesis of Sodium Tetra(8-Hydroxyquinolino)Boron ( $\text{NaBq}_4$ ) and Preparation of Fluorescent Fingerprinting Powders using 8-Hydroxyquinoline Salts

### 3.1 Introduction

$\text{NaBq}_4$  was selected as one of the analogues of  $\text{Alq}_3$  to investigate as a potential fluorescent compound for use in a fingerprinting powder.  $\text{NaBq}_4$  is a salt of  $\text{Na}^+$  and the  $[\text{Bq}_4]^-$  anion.  $[\text{Bq}_4]^-$  is reported<sup>[1]</sup> to be comprised of boron(III) bonded to four deprotonated 8-hydroxyquinoline anions. Unlike the other 8-hydroxyquinoline compounds discussed in this thesis, the bonding to the central atom is monodentate, so the geometry about the boron is tetrahedral. This monodentate bonding means the photophysical properties of  $\text{NaBq}_4$  are expected to be quite different to those of the 8-hydroxyquinoline compounds investigated in Chapter Two.

A modified version of a literature method developed by Wang *et al.*<sup>[1]</sup> to synthesise  $\text{NaBq}_4$  was carried out. This chapter will cover the preparation and characterisation of the products acquired using this method. Considering the reactants used to prepare  $\text{NaBq}_4$ , there is a possibility of a sodium salt of  $[\text{q}]^-$  forming. Examination of the Cambridge Structural Database showed that the salt most likely to form would be  $\text{Na}_4\text{q}_4(\text{H}_2\text{O})_8$ . For comparison purposes, a sample of  $\text{Na}_4\text{q}_4(\text{H}_2\text{O})_8$  was also

prepared using a modified literature method<sup>[2]</sup> and characterised alongside the products of the NaBq<sub>4</sub> synthesis.

Na<sub>4</sub>q<sub>4</sub>(H<sub>2</sub>O)<sub>8</sub> was first prepared and characterised by single crystal X-ray diffraction (XRD) in 2011 by Deacon *et al.*<sup>[2]</sup> The database identifier of the compound in the Cambridge Crystallographic Data Centre (CCDC) is “DAMHOQ”. Each sodium ion is six-coordinate, as it is bonded to a chelating 8-hydroxyquinoline anion and four water molecules. Na<sub>4</sub>q<sub>4</sub>(H<sub>2</sub>O)<sub>8</sub> forms a two-dimensional sheet polymer as the water molecules bridge between adjacent sodium ions (see Fig. 3.1). In addition to being characterised, the products of the NaBq<sub>4</sub> synthesis were also used to make fluorescent fingerprinting powders as per the methods described in Chapter Two.

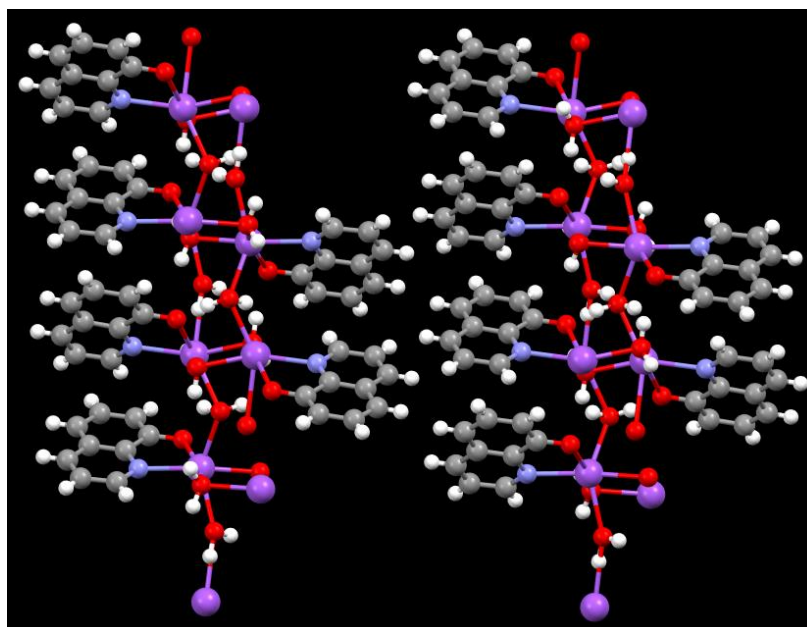


**Figure 3.1:** Structure of Na<sub>4</sub>q<sub>4</sub>(H<sub>2</sub>O)<sub>8</sub>. The elements are colour coded white, grey, blue, red and purple for hydrogen, carbon, nitrogen, oxygen, and sodium, respectively.

## 3.2 Experimental

### 3.2.1 Materials

**Table 3.1:** Chemicals

| <b>Name</b>        | <b>Source</b>                                    |
|--------------------|--|
| Ethanol (absolute) | University of Waikato Science Store (drum grade) |
| Dichloromethane    | Merck (Emsure grade)                             |
| Diethyl ether      | University of Waikato Science Store (drum grade) |
| Sodium borohydride | Aldrich  |
| 8-Hydroxyquinoline | Honeywell Riedel-de Haën AG                      |
| Sodium hydroxide   | Ajax Finechem                                    |
| DMSO               | Aldrich (>99%)                                   |
| d6-DMSO            | Aldrich (99.96% deuterated)                      |
| Acetone            | University of Waikato Science Store (drum grade) |
| Nitric Acid        | Merck (Emsure grade, 65%)                        |
| IV-ICPMS-71A       | Inorganic Ventures (ICP-MS standard)             |

**Table 3.2:** Equipment

| <b>Equipment Type</b>                     | <b>Brand</b>                            |
|---|---|
| X-ray diffractometer (single crystal)     | Agilent Supernova                       |
| X-ray diffractometer (powder diffraction) | PANalytical Empyrean                    |
| NMR Spectrometer                          | Bruker Avance DRX400 FT-NMR             |
| ESI-MS                                    | Bruker Daltonics MicrOTOF™ Spectrometer |
| ICP-MS                                    | Perkin-Elmer SCIEX DRC II               |
| Melting Point Apparatus                   | Büchi M-560                             |
| Melting Point Bar                         | Leica VMHB System Kofler                |
| UV-Vis Spectrophotometer                  | Agilent Cary 100                        |
| Ultraviolet Lamp, 365 nm Tube             | Uvitec                                  |

### 3.2.2 Synthesis of $\text{NaBq}_4$

In a beaker,  $\text{NaBH}_4$  (0.76 g) was dissolved in ethanol (20 mL). A solution of 8-hydroxyquinoline (11.6 g) in ethanol (120 mL) was added dropwise to the  $\text{NaBH}_4$  solution while stirring magnetically. The solution

was left to stir (2 hours). A white precipitate formed as the solution was stirred. The precipitate was filtered and washed with ether (50 mL) on a Büchner funnel. The solid was placed in an oven to dry (20 hours, 50°C). The final weight of the product was 2 g. The product was labelled substance **A**. The synthesis was attempted again using a different batch of  $\text{NaBH}_4$  (from the same supplier) and the purified solid was dried in a desiccator (3 days) before drying in an oven (20 hours, 50°C). The second synthesis produced 9 g of solid. The product was labelled substance **B**. The difference in yield may be explained by the different batch of  $\text{NaBH}_4$  used, as  $\text{NaBH}_4$  degrades to  $\text{NaBO}_2$  and  $\text{H}_2$  if exposed to moisture.<sup>[3]</sup>

### 3.2.3 Synthesis of $\text{Na}_4\text{q}_4(\text{H}_2\text{O})_8$ Crystals

$\text{Na}_4\text{q}_4(\text{H}_2\text{O})_8$  was prepared using a modified literature method.<sup>[2]</sup> 8-Hydroxyquinoline (4.535 g) and sodium hydroxide (1.25 g) were added to a beaker containing ethanol (250 mL). The solution was poured into a three-necked round bottom flask. Through one neck, nitrogen was passed into the flask to remove air, the second neck was left open to avoid pressure build-up, and the third neck was sealed. The flask was wrapped in aluminium foil to exclude light. The solution was allowed to evaporate under a flow of nitrogen (1 week). Some ethanol remained after a week, so the remainder was removed via glass pipette. The sample was again left to dry under a flow of nitrogen (48 hours). The light brown crystals were removed from the flask and weighed. The mass of the product was 0.5 g, which corresponds to a yield of 5%. A greater yield could have been attained by allowing the last portion of ethanol to evaporate.

#### *3.2.4 Preparation of Fluorescent Fingerprinting Powders*

To a round bottom flask (500 mL), magnetite, the fluorescent compound (10 g of material total, see below for ratios), and dichloromethane (150 mL) were added. The fluorescent compound dissolved in the dichloromethane, while the magnetite remained undissolved. The magnetite was coated by the fluorescent compound during rotary evaporation.

Three different powder formulations were prepared. The first contained 20% substance **A** by mass, while the other two powders contained 10% and 20% substance **B** by mass; these powders were given the labels '20% BM', '10% BM2', and '20% BM2', respectively.

#### *3.2.5 Application Method*

For the method used to apply the fingerprinting powders to the test surfaces, refer to section 2.2.7.

#### *3.2.6 Assessment of Powders*

For information on how the performance of the fingerprinting powders was assessed, refer to section 2.2.9.

### *3.2.7 Inductively Coupled Plasma Mass Spectrometry (ICP-MS) Sample Preparation*

To prepare a  $41 \text{ mg L}^{-1}$  solution of substance **A** for ICP-MS analysis, the following method was used: Substance **A** (4.1 mg) and nitric acid (2 mL, 65%) were added to a volumetric flask (100 mL) and made up to the mark with distilled water. The flask was inverted to ensure the solution was mixed. The solution was poured into a beaker (250 mL) and loaded into a syringe fitted with a filter. The filter was removed from the syringe and a portion of the solution (10 mL) was emptied into a falcon tube (15 mL). A  $1.3 \text{ g L}^{-1}$  solution of substance **B** was prepared for ICP-MS analysis in the same manner as detailed above, with the exception that substance **B** (0.13 g) was used in place of substance **A**. Both substances were completely soluble in the acidified solution. The standard used was IV-ICPMS-71A.

### *3.2.8 Electrospray Ionisation Mass Spectrometry (ESI-MS) Experiments*

Samples of substance **A**, substance **B**, and  $\text{Na}_4\text{q}_4(\text{H}_2\text{O})_8$  were dissolved in methanol and analysed by ESI-MS. The voltages of each experiment are abbreviated to capillary voltage/skimmer voltage. Positive ion spectra were acquired at 150/50 V, while the negative ion spectra were acquired at -90/-30 V. An additional experiment was run for  $\text{Na}_4\text{q}_4(\text{H}_2\text{O})_8$  at 90/30 V.

### 3.2.9 Nuclear Magnetic Resonance (NMR) Spectroscopy Experiments

Samples of substance **A**, substance **B**,  $\text{Na}_4\text{q}_4(\text{H}_2\text{O})_8$ , and 8-hydroxyquinoline were dissolved in  $\text{d}_6$ -DMSO for analysis by NMR.

#### Substance **A**

$^1\text{H}$  NMR:  $\delta$  6.77 (d, 1H,  $J=7.7$  Hz), 6.91 (d, 1H,  $J=7.3$  Hz), 7.26 (t, 1H,  $J=7.9$  Hz, 7.6 Hz), 7.37(dd, 1H,  $J=3.7$  Hz, 7.7 Hz), 8.13 (d, 1H,  $J=8.4$  Hz), 8.64 (dd, 1H, br)

$^{13}\text{C}$  NMR:  $\delta$  111.4, 112.5, 121.3, 128.8, 130.3, 136.2, 142.2, 146.6, 161.3

#### Substance **B**

$^1\text{H}$  NMR:  $\delta$  6.95 (dd, 1H,  $J=1.3$ , 7.7Hz), 7.15 (d, 1H,  $J=8.1$  Hz), 7.35 (t, 1H,  $J=7.9$  Hz), 7.46 (dd, 1H,  $J=4.2$  Hz, 8.3 Hz), 8.22 (dd, 1H,  $J=1.7$  Hz, 8.4 Hz), 8.74 (dd, 1H,  $J=1.7$  Hz, 4.2 Hz)

$^{13}\text{C}$  NMR:  $\delta$  112.3, 114.3, 121.7, 128.5, 129.9, 136.3, 140.9, 147.4, 158.2

#### $\text{Na}_4\text{q}_4(\text{H}_2\text{O})_8$

$^1\text{H}$  NMR:  $\delta$  6.75 (d, 1H,  $J=7.7$  Hz), 6.84 (d, 1H,  $J=7.9$  Hz), 7.23 (t, 1H,  $J=7.7$  Hz, 7.8 Hz), 7.34 (dd, 1H,  $J=4.1$  Hz, 8.1 Hz), 8.10 (d, 1H,  $J=8.3$  Hz), 8.61 (dd, 1H,  $J=1.6$  Hz, 4.1 Hz)

$^{13}\text{C}$  NMR:  $\delta$  110.4, 112.7, 121.1, 128.9, 130.5, 136.1, 142.7, 146.3, 162.7

### 8-Hydroxyquinoline

$^1\text{H}$  NMR:  $\delta$  7.09 (dd, 1H,  $J=1.5$  Hz, 7.3Hz), 7.42 (m, overlapping peaks), 7.54 (dd, 1H,  $J=4.1$  Hz, 8.3 Hz), 8.32 (dd, 1H,  $J=1.6$  Hz, 8.3 Hz), 8.85 (dd, 1H,  $J=1.7$  Hz, 4.2 Hz), 9.79 (s, 1H, br)

$^{13}\text{C}$  NMR:  $\delta$  111.7, 118.2, 122.3, 128.0, 129.3, 136.5, 138.9, 148.6, 153.74

#### 3.2.10 UV-Vis Sample Preparation

Samples to be analysed by UV-Vis spectrophotometry were prepared using the following method: To a falcon tube (15 mL), a portion of sample (1 mg) and DMSO (10 mL) were added. The cap was secured and the solution mixed by shaking the tube. To a quartz cuvette, a small amount of solution (0.5 mL) and DMSO (2 mL) was added. The cuvette was then placed in the spectrophotometer for analysis. Samples of substance **A**, substance **B**, and  $\text{Na}_4\text{q}_4(\text{H}_2\text{O})_8$  were prepared in this manner. DMSO was used as the blank solution.

#### 3.2.11 XRD Experiments

The settings used by the X-ray diffractometer for acquiring the powder patterns of substance **A**, substance **B**, and  $\text{Na}_4\text{q}_4(\text{H}_2\text{O})_8$  are detailed in Table 3.3.

**Table 3.3:** Powder Diffractometer Settings

|                                   |  |
|-----------------------------------|--|
| Anode material                    | Cu   |
| K- $\alpha$ 1 wavelength          | 1.540598 Å   |
| K- $\alpha$ 2 wavelength          | 1.544426 Å   |
| Ratio K- $\alpha$ 2/K- $\alpha$ 1 | 0.5  |
| Monochromator used                | -  |
| Generator voltage                 | 45   |
| Tube current                      | 40   |
| h k l                             | 0 0 0  |
| Scan axis                         | Gonio  |
| Scan range                        | 4.981199996-50.98971   |
| Scan step size                    | 0.0525211  |
| No. of points                     | 876  |
| Scan type                         | Continuous   |
| Phi                               | 85 (Substance <b>A</b> ), 322.6 (Substance <b>B</b> ), 282.5 (Na <sub>4</sub> q <sub>4</sub> (H <sub>2</sub> O) <sub>8</sub> ) |
| Time per step                     | 153.255 s  |

### 3.3 Results of Characterisation Experiments

The techniques used to characterise substance **A**, substance **B**, and Na<sub>4</sub>q<sub>4</sub>(H<sub>2</sub>O)<sub>8</sub> include NMR spectroscopy, ESI-MS, UV-Vis absorbance spectroscopy, and melting point measurements. Single crystal XRD was only performed for Na<sub>4</sub>q<sub>4</sub>(H<sub>2</sub>O)<sub>8</sub>, while powder XRD patterns were gathered for all samples.

#### 3.3.1 Physical Properties

Substance **A** was a white solid that formed large, flat aggregates that exhibited a degree of flexibility. An optical microscope was used to determine that the aggregates were made of many small, needle-like

crystals. As a solid, the material emitted bright blue light under UV excitation (365 nm). When dissolved in acetone, the solution fluoresced at a green-yellow wavelength, but when dissolved in DMSO, the solution glowed a slightly redshifted, gold colour. Substance **B** was also a white solid that formed aggregates, though instead of sheets, the aggregates were much more rounded in appearance than the aggregates formed by substance **A**. Substance **B** also fluoresced blue under UV excitation. The  $\text{Na}_4\text{q}_4(\text{H}_2\text{O})_8$  crystals were similar in appearance to 8-hydroxyquinoline, as they were a mixture of brown to colourless, needle-like crystals. The  $\text{Na}_4\text{q}_4(\text{H}_2\text{O})_8$  crystals fluoresced blue under UV excitation. The samples were slow to dissolve in chloroform and even slower in water. Methanol and DMSO dissolved them almost immediately.

### 3.3.2 Melting Point Measurements

Substance **A**, substance **B** and  $\text{Na}_4\text{q}_4(\text{H}_2\text{O})_8$  did not melt on the melting point bar at the limit of the apparatus (260°C). However, all three of the samples turned yellow above 120°C. The yellow substance did not fluoresce under UV light. This shared behaviour suggests that the samples were of similar composition.

Using the Büchi melting point apparatus, the samples were observed to change colour as the temperature was increased. Each sample changed to a yellow colour, darkening to a shade of brown, and then finally decomposed to a soot-like material. Table 3.4 displays the temperature at which each transition occurred for the samples.

**Table 3.4:** Transition temperatures measured by the Büchi apparatus.

| Sample   | Yellow Transition | Brown Transition | Soot Transition |
|--|-------------------|------------------|-----------------|
| Substance <b>A</b>   | 215°C             | 290°C            | 330°C           |
| Substance <b>B</b>   | 170°C             | 180°C            | 200°C           |
| Na <sub>4</sub> q <sub>4</sub> (H <sub>2</sub> O) <sub>8</sub> | 170°C             | 250°C            | 330°C           |

The samples turned yellow at a higher temperature in the Büchi apparatus (170°C *cf.* 120°C). It is speculated that the colour transitions may be dependent on the amount of light or air available, as 8-hydroxyquinoline compounds have been reported to be sensitive to such factors.<sup>[4][5]</sup> The melting point bar allowed for abundant airflow to the samples, while the thin capillary tubes of the Büchi apparatus greatly restricted the airflow and light to the samples. The difference in packing of the powders (due to the shape of the sample particulates) in the tubes may have affected the temperature at which they transitioned if it was dependent on light and/or air.

Substance **A** and Na<sub>4</sub>q<sub>4</sub>(H<sub>2</sub>O)<sub>8</sub> underwent transitions at similar temperatures, which suggests they may be similar chemically or in fact be the same compound. Substance **B** decomposed at a lower temperature than the other samples, which suggests it is not of similar composition to either of them or is of low purity.

The brown colour change observed may be caused by the condensation of 8-hydroxyquinoline from the samples. A study by Papadimitrakopoulos *et al.*<sup>[5]</sup> reported a similar colour change in samples of Alq<sub>3</sub> when heated beyond 150°C in the presence of oxygen.

### 3.3.3 Analysis by ICP-MS

Elemental analysis of the unknown compounds by ICP-MS was used to determine if their stoichiometries matched what would be expected of  $\text{NaBq}_4$ . Analysis of a  $41 \text{ mg L}^{-1}$  solution of substance **A** showed boron levels of 29 ppb, which was approximately 3.8% of the value expected (726 ppb) for a solution of  $\text{NaBq}_4$  at the same concentration. The sodium content was 3398 ppb, which is in contention with the mass ratio of boron to sodium in  $\text{NaBq}_4$ . The mass ratio was expected to be approximately 32:68 boron to sodium, but experimentally was found to be 0.84:99.16 boron to sodium. These results strongly suggest that substance **A** was unlikely to contain anything more than trace amounts of  $\text{NaBq}_4$ . The sodium content was 73% of the expected value for a  $41 \text{ mg L}^{-1}$  solution of  $\text{Na}_4\text{q}_4(\text{H}_2\text{O})_8$ .

Since the substance **A** solution had a very low concentration of boron, the substance **B** solution was made to a much higher concentration ( $1.3 \text{ g L}^{-1}$ ) to ensure that the boron concentration wouldn't be below the detection limit of the instrument.

The concentration of boron in the substance **B** solution was 5128 ppb, which is approximately 22.5% of the expected concentration (22800 ppb) for a solution of  $\text{NaBq}_4$  at the same concentration. Sodium was present in the substance **B** solution at 48315 ppb. This represents a mass ratio of 9.6:90.4 boron to sodium. The boron to sodium ratio in substance **B** makes the presence of  $\text{NaBq}_4$  more plausible; however it would be of low purity. The sodium content was only 33% of the expected value for a  $1.3 \text{ g L}^{-1}$  solution of  $\text{Na}_4\text{q}_4(\text{H}_2\text{O})_8$ .

### 3.3.4 Characterisation by ESI-MS

8-Hydroxyquinoline complexes containing moderately hard metal centres, such as bis(8-hydroxyquinolinato)manganese, are known to readily fragment under electrospray ionisation conditions, with only highly stable compounds, such as bis(8-hydroxyquinolinato)copper, being detectable in positive ion mode.<sup>[6][7]</sup> The expected ions for NaBq<sub>4</sub> are Na<sup>+</sup> and [Bq<sub>4</sub>]<sup>-</sup>. The Na<sup>+</sup> cation would give rise to a signal at *m/z* 23 and the [Bq<sub>4</sub>]<sup>-</sup> anion would give rise to a signal at *m/z* 587, provided it is stable under electrospray conditions.

The positive ion mass spectrum of substance **A** gave strong peaks at *m/z* 190, 357, 381, 524, 578, 647, 691, and 789. All of these peaks have isotope patterns that are reminiscent of organic compounds that contain carbon, hydrogen, oxygen, and nitrogen. While the majority of the peaks could not be assigned, the peak at *m/z* 357 was suspected to correspond to the [Na<sub>3</sub>q<sub>2</sub>]<sup>+</sup> cation (see Fig. 3.2). The occurrence of ion clusters, such as [Na<sub>3</sub>q<sub>2</sub>]<sup>+</sup>, is common in the spectra of ionic salts.<sup>[8]</sup>

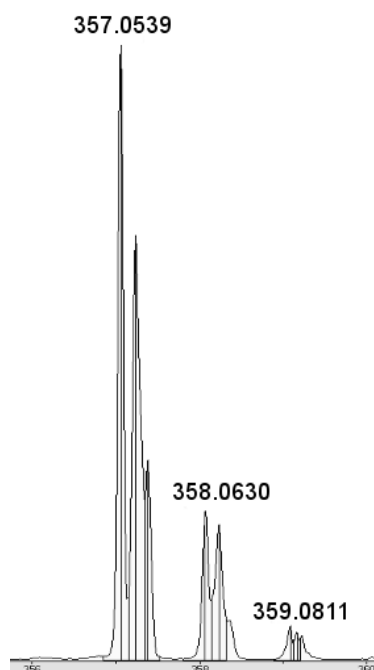


**Figure 3.2:**  $m/z$  357 peak in the positive ion ESI mass spectrum of substance **A**. Note that the doubling of peaks was an artefact caused by the instrument.

The negative ion spectrum of substance **A** was dominated by a peak at  $m/z$  144, which was the deprotonated 8-hydroxyquinoline anion,  $[q]^-$  (see Fig. 3.3). A much less intense peak at  $m/z$  311 was also present, corresponding to the  $[Naq_2]^-$  anion. In agreement with the results from the ICP-MS analysis, the characteristic boron isotope pattern (approximately 20%  $^{10}B$  and 80%  $^{11}B$ ) was absent from all ions in the spectrum.



**Figure 3.3:** Main peaks of the negative ion ESI mass spectrum of substance **A**.

The positive ion mass spectrum of substance **B** also had the  $m/z$  190, 357, 381, 524, 578, and 691 peaks that were present in the positive ion mass spectrum of substance **A**. In the substance **A** spectrum, the  $m/z$  381 peak was roughly 60% of the intensity of the  $m/z$  190 peak, but in the substance **B** spectrum, it was only about 5%. Much like the substance **A** spectrum, the dominant peaks of the negative ion mass spectrum of substance **B** were at  $m/z$  144 and 311.

The positive ion mass spectrum (150/50 V) of  $\text{Na}_4\text{q}_4(\text{H}_2\text{O})_8$  shared more in common with that of substance **A** than of substance **B**, as they both had peaks at  $m/z$  190, 357, 381, 524, 647, 691, and 789. Reducing the voltages to 90/30 V caused the  $m/z$  168 peak to become dominant

(see Fig. 3.4). This peak was likely the  $[\text{NaHq}]^+$  cation, which is an adduct formed from  $\text{Na}^+$  and the neutral 8-hydroxyquinoline molecule. The negative ion mass spectrum of  $\text{Na}_4\text{q}_4(\text{H}_2\text{O})_8$  was very similar to that of substances **A** and **B** as it showed a dominant  $[\text{q}]^-$  peak and a less intense  $[\text{Naq}_2]^-$  peak.

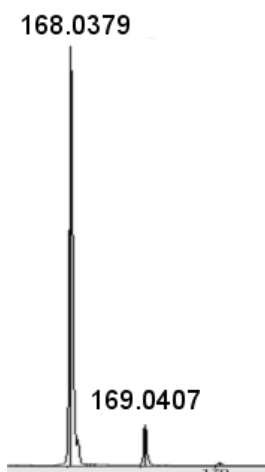


**Figure 3.4:**  $m/z$  168 peak in the positive ion ESI mass spectrum of  $\text{Na}_4\text{q}_4(\text{H}_2\text{O})_8$  (90/30 V).

### 3.3.5 Characterisation by NMR

The  $^1\text{H}$  and  $^{13}\text{C}$  NMR spectra of substance **A**, substance **B**, and  $\text{Na}_4\text{q}_4(\text{H}_2\text{O})_8$  were acquired. The  $^1\text{H}$  and  $^{13}\text{C}$  NMR spectra of 8-hydroxyquinoline were also acquired for comparison purposes. As expected with  $d_6$ -DMSO, the peaks in all the spectra were fairly broad. The samples of substance **A**, substance **B**, and  $\text{Na}_4\text{q}_4(\text{H}_2\text{O})_8$  formed bright yellow solutions that gradually turned brown, then to dark red over a period of several days. As the colour changed, small, sharp peaks began to appear in the  $^1\text{H}$  NMR spectra of these compounds. This suggested the

colour change was due to slow decomposition of the compounds. The intensity and sharpness of the water peak also changed over time. This was likely due to water entering the sample, as d6-DMSO is hygroscopic. The 8-hydroxyquinoline sample formed a slightly pink solution that did not change colour over time. To avoid any issues associated with increasing water concentration or potential decomposition, all experiments were run using fresh samples. The  $^1\text{H}$  NMR spectra (6.5 ppm to 9 ppm) of the substances are compared in Fig. 3.5.

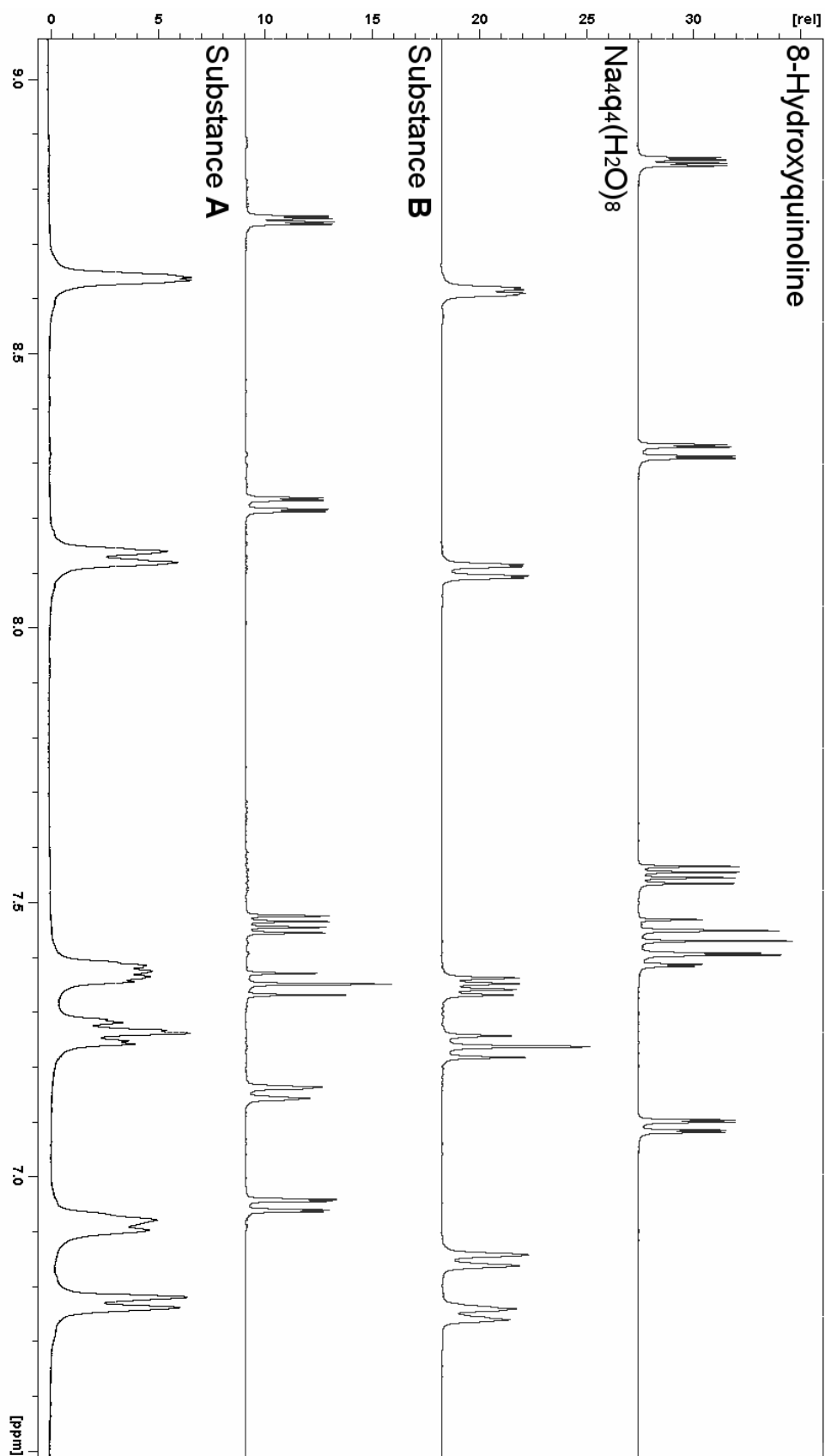


**Figure 3.5:**  $^1\text{H}$  NMR spectra (6.5 ppm to 9 ppm) of substance **A**, substance **B**,  $\text{Na}_4\text{q}_4(\text{H}_2\text{O})_8$  and 8-hydroxyquinoline.

The similarity of the  $^1\text{H}$  and  $^{13}\text{C}$  NMR spectra of substance **A**, substance **B**, and  $\text{Na}_4\text{q}_4(\text{H}_2\text{O})_8$  was expected, as their syntheses all involved the formation of an 8-hydroxyquinoline compound, with no major modification to the ligand. There are three main differences between the  $^1\text{H}$  NMR spectra of the aforementioned compounds and the  $^1\text{H}$  NMR spectrum of 8-hydroxyquinoline (shown in Fig. 3.6).

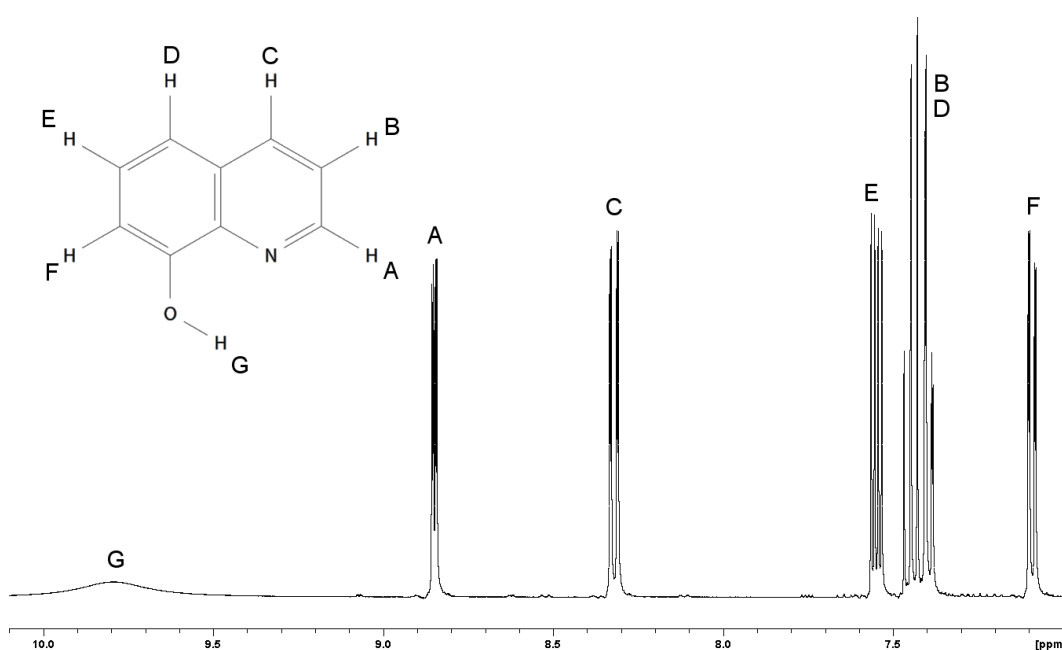


**Figure 3.6:**  $^1\text{H}$  NMR spectrum of 8-hydroxyquinoline. The peak assignments are in agreement with literature values.<sup>[9]</sup>

The first difference is the set of overlapping peaks at  $\delta$  7.42 in the  $^1\text{H}$  NMR spectrum of 8-hydroxyquinoline. The overlapping peaks were not present in the other spectra; this was most likely due to changes in chemical shift in the other compounds that caused the peaks to separate.

The next distinguishing feature of the  $^1\text{H}$  NMR spectrum of 8-hydroxyquinoline was the presence of a broad peak at  $\delta$  9.79. This peak was attributed to the proton attached to the oxygen atom. This proton was not present in the other substances because it was removed from the 8-hydroxyquinoline molecule during their preparation by addition of base. Lastly, the peaks in the  $^1\text{H}$  NMR spectrum of 8-hydroxyquinoline were noticeably further downfield.

The  $^1\text{H}$  and  $^{13}\text{C}$  NMR spectra of substance **A** and  $\text{Na}_4\text{q}_4(\text{H}_2\text{O})_8$  were very similar in terms of chemical shifts (see Fig. 3.7).

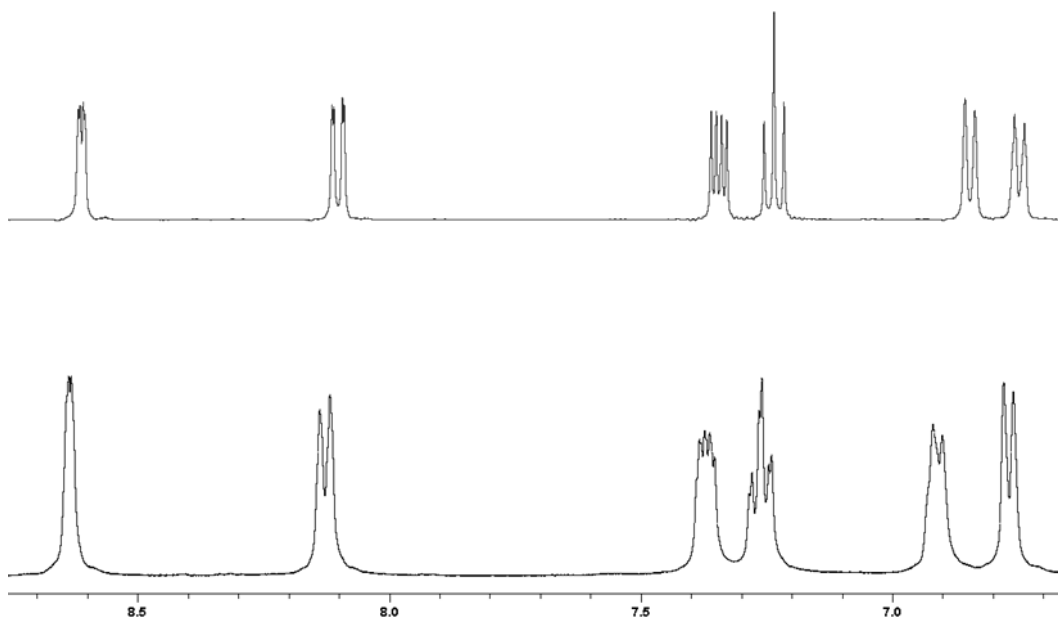


**Figure 3.7:** Partial  $^1\text{H}$  NMR spectra of  $\text{Na}_4\text{q}_4(\text{H}_2\text{O})_8$  (top) and substance **A** (bottom).

The peak at  $\delta$  8.64 in the  $^1\text{H}$  NMR spectrum of substance **A** was very broad with noticeable shoulder peaks, making its coupling constants impossible to determine with confidence, but given that the  $\delta$  8.61 peak in

the  $^1\text{H}$  NMR spectrum of  $\text{Na}_4\text{q}_4(\text{H}_2\text{O})_8$  was a doublet of doublets, the substance **A** peak has also been labelled a doublet of doublets. Fig. 3.8 provides a close up view of the peaks in question.

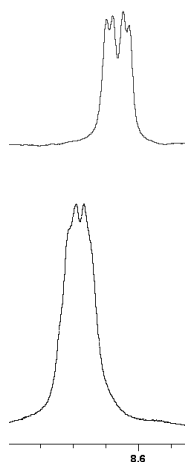


**Figure 3.8:**  $\delta$  8.61 peak in the  $^1\text{H}$  NMR spectrum of  $\text{Na}_4\text{q}_4(\text{H}_2\text{O})_8$  (top) and  $\delta$  8.64 peak in the  $^1\text{H}$  NMR spectrum of substance **A** (bottom).

### 3.3.6 UV-Vis Absorbance Experiments

The UV-Vis absorption spectra of substance **A**, substance **B**, and  $\text{Na}_4\text{q}_4(\text{H}_2\text{O})_8$  were acquired. Considering that all the compounds fluoresced a similar colour and contained 8-hydroxyquinoline, their Stokes shifts were expected to be very close. The Stokes shift is the difference in wavelength between the absorption and emission of an electronic transition.<sup>[10]</sup> These factors mean that it was expected that the compounds would give similar absorption spectra (see Fig. 3.9).

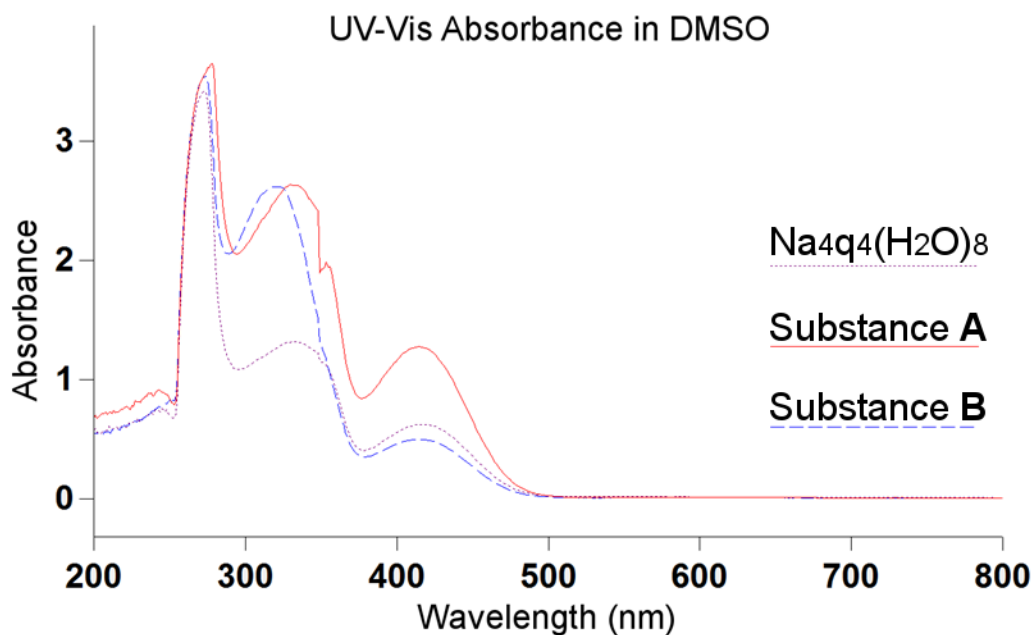


**Figure 3.9:** Graph showing the UV-Vis absorbances of substance **A**, substance **B**, and  $\text{Na}_4\text{q}_4(\text{H}_2\text{O})_8$

The wavelengths of the maximum absorbances of substance **A**, substance **B**, and  $\text{Na}_4\text{q}_4(\text{H}_2\text{O})_8$  were 278 nm, 274 nm, and 273 nm, respectively. Taking into account the results of the NMR experiments, it was unexpected that the maximum absorbance of substance **B** was closer than substance **A** to that of  $\text{Na}_4\text{q}_4(\text{H}_2\text{O})_8$ . The wavelengths of the second highest absorbances were more in line with predictions as they were 330 nm, 321 nm, and 331 nm for substance **A**, substance **B**, and  $\text{Na}_4\text{q}_4(\text{H}_2\text{O})_8$ , respectively.

### 3.3.7 XRD Results

The single crystal XRD of  $\text{Na}_4\text{q}_4(\text{H}_2\text{O})_8$  was carried out to confirm the composition of the sample. The crystal structure solved for this thesis has been deposited in the CCDC as “DAMHOQ01” because the R factor was superior to that of “DAMHOQ” (4.5% *cf.* 11%, see Appendix II for crystal data).

Attempts to grow large crystals of substances **A** and **B** by slow evaporation for single crystal XRD failed, as the compounds would decompose and crystals of 8-hydroxyquinoline would grow instead. This was confirmed by single crystal XRD. The powder XRD patterns of substances **A** and **B** (see Fig. 3.10) were acquired to compare to the powder pattern of  $\text{Na}_4\text{q}_4(\text{H}_2\text{O})_8$  (see Fig. 3.11).

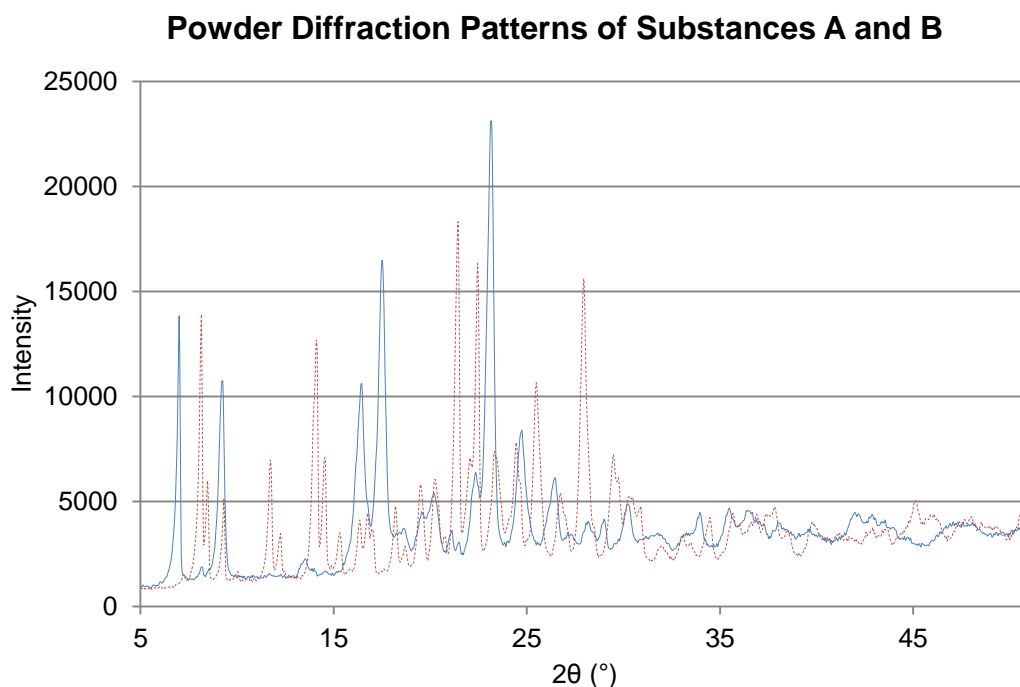


**Figure 3.10:** Powder diffraction patterns of substance **A** (solid) and substance **B** (dashed).

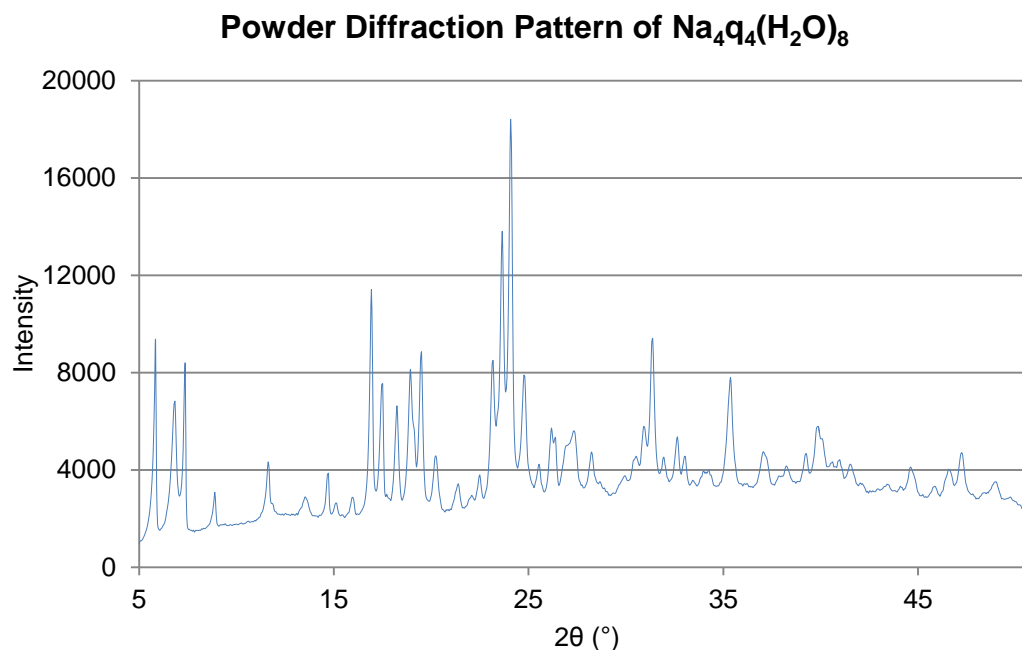


**Figure 3.11:** Powder diffraction pattern of  $\text{Na}_4\text{q}_4(\text{H}_2\text{O})_8$ .

None of the powder patterns resembled each other. This was unexpected as the data from the other experiments implied the samples were of similar composition. However, these results do not rule out the possibility of the samples containing different crystalline forms of the same compound, as polymorphs or different hydrates may give very different powder patterns.

### 3.4 Characterisation Discussion

The results of the ICP-MS analyses (*vide supra*) made a strong case against the unknown samples containing much  $\text{NaBq}_4$ . Some  $\text{NaBq}_4$  may have been present, but only in small amounts. Substance **B** was determined to have a significantly higher boron content than substance **A**,

but not enough to suggest that  $\text{NaBq}_4$  was the main component. The low sodium content of substance **B** implied it was of low purity. Crystals of  $\text{Na}_4\text{q}_4(\text{H}_2\text{O})_8$  were synthesised to act as a standard to which substances **A** and **B** could be compared to. The composition of the  $\text{Na}_4\text{q}_4(\text{H}_2\text{O})_8$  was confirmed by using single crystal XRD to solve its structure and comparing that to the structure solved by Deacon, *et al.*<sup>[2]</sup> The powder patterns of substances **A** and **B** were different from the pattern of  $\text{Na}_4\text{q}_4(\text{H}_2\text{O})_8$ , confirming that the samples did not share the same polymorph.

An attempt to find the melting points of the samples was made, but they all decomposed before melting. The samples underwent colour changes as the temperature was increased, with substance **A** and  $\text{Na}_4\text{q}_4(\text{H}_2\text{O})_8$  changing colours at comparable temperatures. This suggests that substance **A** may contain a significant amount of a species related to  $\text{Na}_4\text{q}_4(\text{H}_2\text{O})_8$ .

Due to the instability of the compounds under electrospray conditions, ESI-MS could not be used to outright confirm the presence of  $\text{NaBq}_4$  or  $\text{Na}_4\text{q}_4(\text{H}_2\text{O})_8$ , but some fragments and adducts of sodium and 8-hydroxyquinoline were detected. The mass spectra of substance **A**, substance **B**, and  $\text{Na}_4\text{q}_4(\text{H}_2\text{O})_8$  were all fairly similar in both positive and negative ion modes. This suggests that they all contained salts of  $\text{Na}^+$  and  $[\text{q}]^-$ . The positive ion mass spectra of substance **A** and  $\text{Na}_4\text{q}_4(\text{H}_2\text{O})_8$  shared more peaks in common with each other than with substance **B**, which is in agreement with the hypothesis that the compositions of substance **A** and  $\text{Na}_4\text{q}_4(\text{H}_2\text{O})_8$  are comparable.

With only  $^1\text{H}$  and  $^{13}\text{C}$  NMR experiments available, only information regarding the nature of the ligand could be acquired from NMR techniques. The spectra of 8-hydroxyquinoline were compared to those of the samples and found to be closely related, with the exception of a few features that were consistent with 8-hydroxyquinoline compounds. The chemical shifts of the compounds were found to be very close, with substance **A** and  $\text{Na}_4\text{q}_4(\text{H}_2\text{O})_8$  having chemical shifts that differed by usually no more than 0.03 ppm. The UV-Vis experiments showed the samples had very similar absorption spectra, with only minor differences in the wavelengths of absorption maxima.

### 3.5 Fingerprinting Powder Performance

Despite the fact that the exact composition of substances **A** and **B** could not be determined, both substances fluoresced brightly enough to be considered for use in fluorescent fingerprinting powders. The powders were tested in the same manner as those in Chapter Two. Table 3.5 details the experimental conditions of each test, as was described in section 2.3.

**Table 3.5:** Conditions of Fingerprinting Tests<sup>2</sup>

| Label     | Formulation Used | Brush    | Surface | UV  | Visible |
|-----------|------------------|----------|---------|-----|---------|
| <b>38</b> | 20% BM           | Zephyr   | C       | 4   | 0.5     |
| <b>39</b> | 20% BM           | Magnetic | C       | 0.5 | 2       |
| <b>40</b> | 20% BM           | Zephyr   | OHP     | 1   | 2       |
| <b>41</b> | 20% BM           | Zephyr   | MS      | 2   | 1       |
| <b>42</b> | 20% BM2          | Zephyr   | C       | 2   | 2       |

<sup>2</sup> The formulation labels are explained in section 3.2.4, while the surfaces and other details are explained in section 2.3.

|    |         |        |     |     |     |
|----|---------|--------|-----|-----|-----|
| 43 | 10% BM2 | Zephyr | C   | 2   | 3   |
| 44 | 20% BM2 | Zephyr | OHP | 0.5 | 1   |
| 45 | 10% BM2 | Zephyr | OHP | 1   | 2   |
| 46 | 20% BM2 | Zephyr | MS  | 2   | 2   |
| 47 | 10% BM2 | Zephyr | MS  | 3   | 2   |
| 48 | 20% BM2 | Zephyr | RP  | 0   | 0.5 |
| 49 | 10% BM2 | Zephyr | RP  | 0   | 0   |
| 50 | 20% BM  | Zephyr | RP  | 0   | 0   |

### 3.5.1 Effects of Powder Formulation

Substance **A** and substance **B** have strong, blue fluorescence. The 20% BM powder caused minimal background staining and had good performance under UV light, but fingerprints visualised by it were difficult to see under visible light. The BM2 powders generally did not perform as well as the 20% BM powder, as they had increased background staining and details of the fingerprints were harder to resolve. Performance-wise, the BM2 powders were very similar to the 20% MgM powder (see Chapter Two).

### 3.5.2 Effects of Test Surface

Unlike the results of Chapter Two, the quality grades of the fingerprints visualised on drink cans were not significantly higher than those visualised on microscope slides. However, the OHP sheets and receipt paper were found to give especially poor results.

The 20% BM powder applied to a can via zephyr brush gave the best result of this chapter with a quality grade of 4 (see Fig. 3.12).

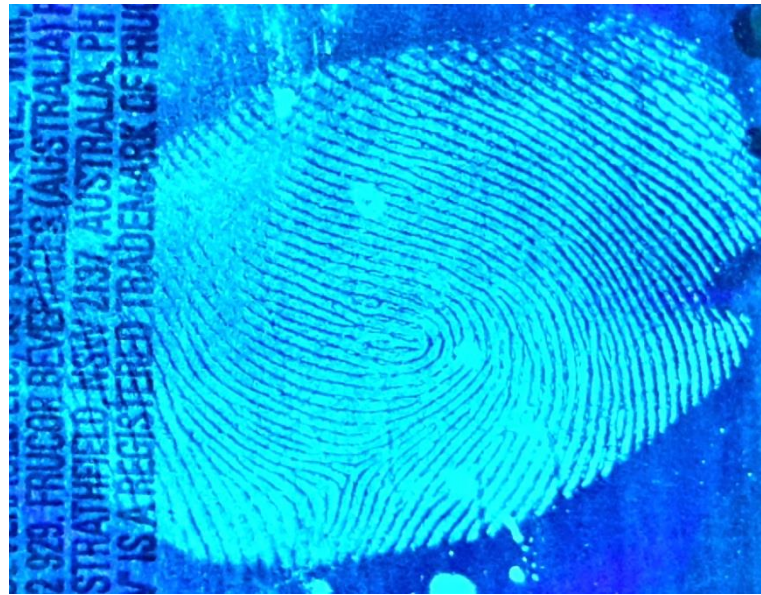


**Figure 3.12:** Fingerprint visualised by 20% BM applied via zephyr brush under UV light.

The 10% BM2 powder in test **47** gave the highest quality grade (3) with a microscope slide as the test surface in the study, equal to 20% AM in test **9** (20% AM powder applied to a microscope slide via zephyr brush). This was an unexpected result, as the quality grade for the 10% BM2 powder was higher on the microscope slide (see Fig. 3.13) than it was for the drink can. The receipt paper gave exceptionally poor results, as the majority of the fingerprints were invisible under both visible and UV light.

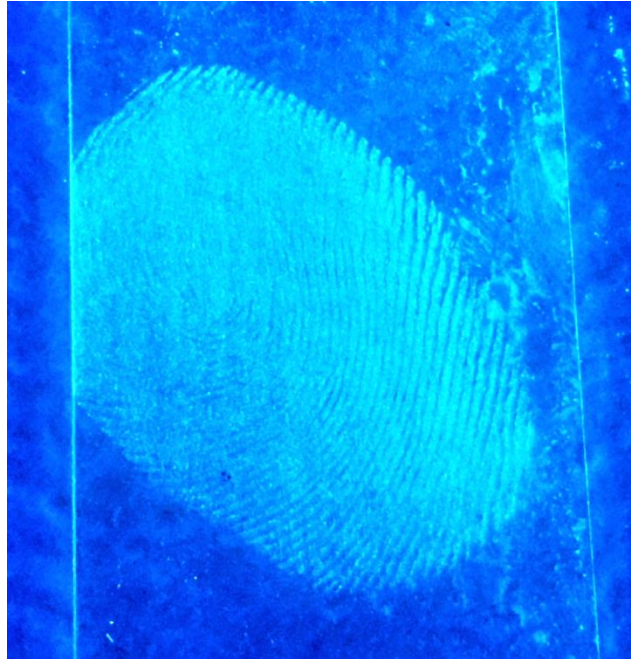


**Figure 3.13:** Fingerprint visualised by 10% BM2 applied via zephyr brush under UV light.

### *3.5.3 Effects of Application Method*

The different brushes had a dramatic effect on the quality of the visualised fingerprints. The zephyr brush was clearly the superior applicator, as the magnetic brush smeared heavily (see Fig. 3.14).



**Figure 3.14:** Attempted visualisation of fingerprint by 20% BM applied via magnetic brush under UV light.

The magnetic brush did not cause heavy background staining as expected after the results of Chapter Two. However, it did leave intense smears that obscured details of the fingerprint. The magnetic brush also did not apply powder to the entirety of the print.

### 3.6 Conclusion

Taking into account the findings from each characterisation experiment performed, it is quite possible that substance **A** contained a significant amount of a  $\text{Na}_4\text{q}_4(\text{H}_2\text{O})_8$  polymorph and possibly some boron compound. The composition of substance **B** was less certain. While it was shown to have properties like that of  $\text{Na}_4\text{q}_4(\text{H}_2\text{O})_8$ , substance **B** differed in

several ways; most notably in the melting point and NMR experiments. It is likely that substance **B** also contained a salt of  $\text{Na}^+$  and  $[\text{q}]^-$ , but not necessarily the same salt that was present in substance **A**. A significant amount of boron in substance **B** was detected by ICP-MS, which suggests that it may contain appreciable amounts of a boron complex.

The trends observed in Chapter Two regarding test surface and application method were mirrored by the results of the experiments in this chapter, as the drink can proved to be the better dusting surface and the zephyr brush was demonstrated to be the superior powder applicator. The 20% BM powder performed the best out of the powders tested in this chapter, as it gave results comparable to that of the 20% AM powder (see Chapter Two).

### 3.7 References

1. Z. Wang, Z. Kang, E. Wang, Z. Su, L. Xu "Intercalation and Photophysical Properties of the Tetra-(8-hydroxyquinolinato) Boron Complex and 3,3',4,4'-Benzophenone Tetracarboxylic Anion into Mg-Al Layered Double Hydroxides" *Inorg. Chem.*, 45, **2006**, 4364-4371
2. G. B. Deacon, T. Dierkes, M. Hübner, P. C. Junk, Y. Lorenz, A. Urbatsch "Alkali Metal/Lanthanoid Heterobimetallic Complexes of 8-Hydroxyquinolinolines Accessed by Pseudo-Solid-State Reactions" *Eur. J. Inorg. Chem*, **2011**, 4338-4348

3. W. Chen, L. Z. Ouyang, J. W. Liu, X. D. Yao, H. Wang, Z. W. Liu, M. Zhu "Hydrolysis and regeneration of sodium borohydride ( $\text{NaBH}_4$ ) – A combination of hydrogen production and storage" J. Power Sources 359, **2017**, 400-407
4. G. Baldacchini, T. Baldacchini, A. Pace, R. B. Podes "Emission Intensity and Degradation Process of  $\text{Alq}_3$  Films" Electrochem. Solid State Lett. 8, **2005** 24-26
5. F. Papadimitrakopoulos, X. M. Zhang, D. L. Thomsen, K. A. Higginson "A Chemical Failure Mechanism for Aluminium(III) 8-Hydroxyquinoline Light-Emitting Devices" Chem. Mater. 8, **1996**, 1363-1365
6. A. R. S. Ross, M. G. Ikonomou, K. J. Orians "Electrospray ionization of alkali and alkaline earth metal species. Electrochemical oxidation and pH effects" J. Mass Spectrom. 35, **2000**, 981-989
7. A. R. S. Ross, M. G. Ikonomou, J. A. J. Thompson, K. J. Orians "Determination of Dissolved Metal Species by Electrospray Ionization Mass Spectrometry" Anal. Chem. 70, **1998**, 2225-2235
8. C. Hao, R. E. March, T. R. Croley, J. C. Smith, S. P. Rafferty "Electrospray ionization tandem mass spectrometric study of salt cluster ions. Part 1 – Investigations of alkali metal chloride and sodium salt cluster ions" J. Mass Spectrom. 36, **2001**, 70-96
9. F. Doğan, İ. Kaya, K. Temizkan "Chemical Oxidative Synthesis and Characterization of Poly(8-hydroxyquinoline) Particles" J.

Macromol. Sci., Part A: Pure and Applied Chemistry 51, **2014**, 948–  
961

10.J. R. Lakowicz *Principles of Fluorescence*, Springer Science &  
Business Media USA, **2007**, 5

## Chapter Four: Concluding Remarks

Of all the fingerprinting powder formulations investigated, those that utilised  $\text{Alq}_3$ ,  $\text{Znq}_2$ , or substance **A** showed the most potential. While substance **A** was suspected to be mainly composed of  $\text{Na}_4\text{q}_4(\text{H}_2\text{O})_8$ , it was not confirmed. For this reason, it would be worth preparing a fingerprinting powder using  $\text{Na}_4\text{q}_4(\text{H}_2\text{O})_8$  as the fluorescent component and comparing its performance to that of the powder made with substance **A** (20% BM).

The powders that consisted of 1:9 and 1:4 parts fluorescent compound to magnetite by mass had the best balance of bright fluorescence and selectivity for fingerprints (with the exception of  $\text{Mgq}_2$  and substance **A**, as powders with a 1:9 ratio were not prepared with these compounds). However, it is difficult to guarantee which ratio gives superior results due to the relatively limited number of experiments. As well as gathering more data to elucidate this matter, experiments involving powders with ratios between 1:9 and 1:4 could be performed to find the ideal ratio.

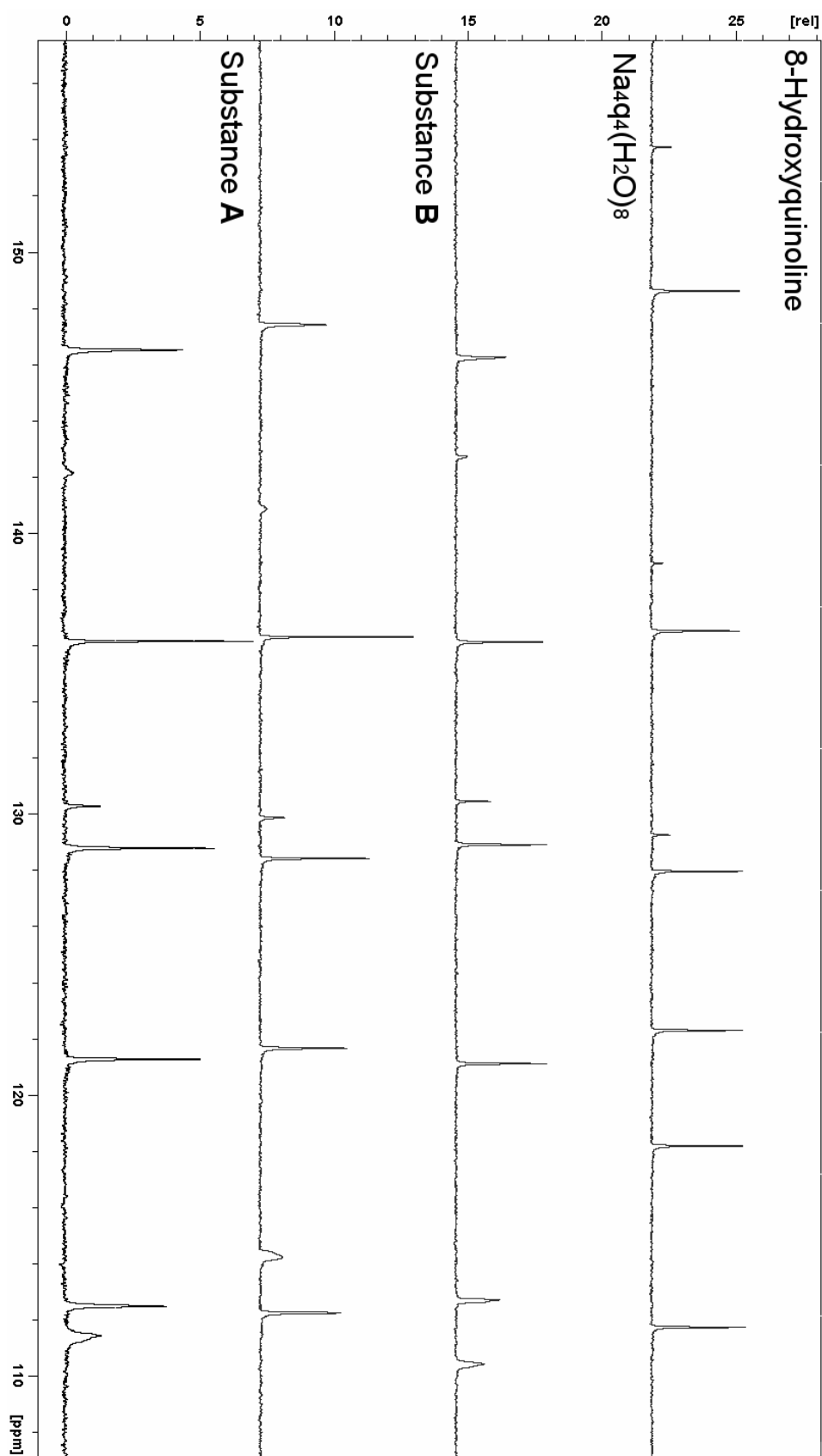
Newer fingerprinting techniques, such as those that employ quantum dots, can visualise the smallest details of a fingerprint by using particles that are only several nanometres in diameter. Taking this into account, it was very unexpected that the fingerprinting powders with the larger particle sizes gave the best results. In order to optimise these powders, a more in-depth study into the relationship between quality of visualised fingerprint and particle size would be quite useful. The method

used in this thesis to divide the powder particles by size was not particularly strict, as the particles were separated into fairly broad size ranges. Employing narrower size ranges (e.g. 10  $\mu\text{m}$  instead of  $\sim 60 \mu\text{m}$ ) may yield different results.

Fingerprinting reagents do not give the same results on every surface, so it is critical to test the reagents on a range of materials. Four smooth, non-porous materials were tested in this thesis, so further experiments should investigate more irregular surfaces, such as wood or fabric.

Lastly, the emission spectra of the fluorescent compounds were never collected. This information would be especially useful in the case of  $\text{Na}_4\text{q}_4(\text{H}_2\text{O})_8$ , as it has not been characterised by this method before. The atmospheric stability tests did not involve anything further than checking to see if the compounds still fluoresced after being exposed to air and light for an extended period. These experiments could be improved by checking the intensity of the emission spectra of each sample before exposure and at specific time intervals after exposure.

Appendix I:  $^{13}\text{C}$  NMR Spectra of Substance A, Substance B,  
 $\text{Na}_4\text{q}_4(\text{H}_2\text{O})_8$ , and 8-Hydroxyquinoline



**Appendix II: Na<sub>4</sub>q<sub>4</sub>(H<sub>2</sub>O)<sub>8</sub> Crystal Data (DAMHOQ01)**

|   |   |
|---|---|
| Empirical formula                           | C <sub>18</sub> H <sub>20</sub> N <sub>2</sub> Na <sub>2</sub> O <sub>6</sub> |
| Formula weight                              | 406.35 g mol <sup>-1</sup>  |
| Temperature/K                               | 100.00(10)  |
| Crystal system                              | monoclinic  |
| Space group                                 | P2 <sub>1</sub> /c  |
| a/Å   | 9.6242(2)   |
| b/Å   | 6.26418(13)   |
| c/Å   | 30.2852(6)  |
| β/°   | 93.4550(19)   |
| Volume/Å <sup>3</sup>                       | 1822.51(7)  |
| Z   | 4   |
| ρ <sub>calc</sub> /g/cm <sup>3</sup>        | 1.4808  |
| μ/mm <sup>-1</sup>                          | 1.335   |
| F(000)                                      | 851.8   |
| Crystal size/mm <sup>3</sup>                | 0.076 × 0.063 × 0.042   |
| Radiation                                   | Cu Kα (λ = 1.54184 Å)   |
| 2θ range for data collection/°              | 9.2 to 147.58   |
| Index ranges                                | -11 ≤ h ≤ 9, -7 ≤ k ≤ 7, -37 ≤ l ≤ 37   |
| Reflections collected                       | 10299   |
| Independent reflections                     | 3578 [R <sub>int</sub> = 0.0376, R <sub>sigma</sub> = 0.0360]                 |
| Data/restraints/parameters                  | 3578/0/285  |
| Goodness-of-fit on F <sup>2</sup>           | 1.053   |
| Final R indexes [I ≥ 2σ (I)]                | R <sub>1</sub> = 0.0439, wR <sub>2</sub> = 0.1164                             |
| Final R indexes [all data]                  | R <sub>1</sub> = 0.0548, wR <sub>2</sub> = 0.1298                             |
| Largest diff. peak/hole / e Å <sup>-3</sup> | 0.50/-0.35  |

Appendix III: Crystal Structure of  $\text{Na}_4\text{q}_4(\text{H}_2\text{O})_8$  (DAMHOQ01)

